Final Report
U.S. Department of Energy

New Silicotitanate Waste Forms: Development and Characterization

Principal Investigator: Dr. Mari Lou Balmer
Pacific Northwest National Laboratory

Co-Investigator: Dr. Tina Nenoff
Sandia National Laboratories

Co-Investigator: Prof. Alexandra Navrotsky
University of California-Davis, Davis, CA 95616

Co-Investigator: Dr. Yali Su
Pacific Northwest National Laboratory

Contributors and Collaborators: Bob Roth (NIST), Hongwu Xu (UC Davis), May Nyman (SNL), Dave McCready (PNNL), Rod Ewing (University of Michigan)

Project Number: 27601

Table of Contents

I. Executive Summary

Research performed on the program "New silicotitantate Waste Forms: Development and Characterization," in the last three years has fulfilled the objectives of the proposal which were to 1.) establish an alternate waste form for disposing of Cs-loaded CSTs in-situ with minimal additives and a final composition similar to the CST, 2.) characterize the phase relationships, structures and thermodynamic and kinetic stabilities of promising waste forms, and 3.) establish a sound technical basis for understanding key waste form properties based on an in-depth understanding of waste form structures and thermochemistry. In addition, a novel class of molecular sieve ion exchangers that show high selectivity for high valence (divalent and trivalent) cations was discovered and the effect of radiation on the stability of select waste forms was determined.

A collaboration between researchers from three institutions, Pacific Northwest National Laboratory, Sandia National Laboratory, and UC Davis was formed to perform the primary work on the program. The unique expertise of each of the members in the areas of waste form development, structure/property relationships, hydrothermal and high temperature synthesis, crystal growth, and thermochemistry was critical to program success. In addition, collaborations with the University of Michigan, SUNY, Stony Brook, SSRL, University of Aberdeen and CSIRO were established to perform radiation stability studies, and crystal structure analysis.

This work has had a significant impact in a number of areas. First, the studies of the thermal stability of the silicotitanate ion exchanger (IE-911) provided an important technical foundation for assessment the viability of this ion exchanger for Cs removal at Savannah River. As a result, an EM-funded, mission directed, joint interaction between the researchers on this program and

the end users of the ion exchanger at Savannah River site has been established. This new program, which is funded by EM, will assess low temperature effects on ion exchanger performance, stability, and phase selection. The DOE will use information from this program to assist in selection of the best process for Cs separation at Savannah River. In addition, data from the study can be used by SRS to develop engineering solutions for potential process upsets. Second, the new class of ion exchangers that were discovered on this program are highly selective for divalent and trivalent cations, thus providing an alternative for removing strontium and actinides from mixed wastes. Finally, we have developed a foundation for understanding structure/property relationships in silicotitanates that can be used to develop more effective materials.

II. Research Objectives

The objective of this program is to identify new waste forms and disposal strategies specific to crystalline silicotitanate (CST) secondary waste generated from Cs and Sr ion exchange processes. Waste forms developed in this work will offer an alternative to current disposal plans. The goals of the program are to reduce the costs associated with CST waste disposal, to minimize the risk of contamination to the environment during CST processing, and to provide DOE with technical alternatives for CST disposal. The technical objectives of the proposed work are to fully characterize the phase relationships, structures, and thermodynamic and kinetic stabilities of CST waste forms and to establish a sound technical basis for understanding key waste form properties such as melting temperatures and aqueous durability, based on an in-depth understanding of waste form structures and thermochemistry.

III. Methods and Results

The methods and results section is organized to summarize progress in several major areas. In the first section the durability of waste forms from the thermally treated ion exchanger (IE-911) is discussed. This is followed by stable and metastable phase selection studies on thermally converted IE-911 and on model systems that are components of the ion exchanger. In this same section, crystal structure studies and structure property relationships are summarized and the properties of a new ion exchanger are discussed. Finally results from high temperature reaction calorimetry to determine thermodynamic parameters are presented followed by a brief discussion of the radiation stability of IE-911 and the Cs-containing phase.

1. Durability of Thermally Converted CST

The durabilities of several of Cs-loaded, thermally converted CST waste forms have been measured. [1-2] The UOP CSTs, designated IE-911, were ion exchanged for 5 and 12 wt% Cs using two methods. In the first method, as-received IE-911 was exchanged for Cs using CsOH solutions. In the second method, IE-911 was pre-treated with NaOH solution until the pH of the eluting solution was higher than 12.5, then exchanged using CsOH solution. Pretreatment of NaOH is recommended by UOP. While the maximum loading on the CST is likely to be only 5 wt% Cs, samples were loaded to 12 wt% Cs to exaggerate potential Cs loss during leaching and to facilitate phase identification of Cs-containing compounds. The Cs-exchanged materials were heat-treated to temperatures ranging from 500°C to 1000°C, analyzed by XRD for phase selection, then characterized for chemical durability. Chemical durability was measured using the standard product consistency test (PCT) and the MCC-1 leach test. The PCT test, which specifies the use of powders in solution, can yield high solution concentrations of leached elements and concomitant reduction of dissolution rates to yield unrealistically high durabilities. The MCC-1 test suspends a pellet in solution and yields conservative durabilities because solution concentrations of the elements are comparatively low, and leaching continues during the entire leach period.

Figure 1 shows the PCT aqueous leach rate of Cs as a function of time for IE-911 that was Na-exchanged, 12 wt% Cs-exchanged, and heat-treated over a range of temperatures. The leach rates were extremely low, ranging from 10^{-8} to 0.002 g/m^2•day. The untreated, 500°C and 900°C treatments exhibited the lowest Cs leach rates, and the total fraction of Cs released for these

samples was less than 1wt% after 7 days. These thermally converted waste forms are several orders of magnitude more durable than borosilicate glass. Standard engineering assessment (EA) borosilicate glass shows a 7-day leached concentration of alkali of 13.3 g/L (there is no Cs in this standard, only Na).[3] In comparison, IE-911 heat-treated to 900°C has a 7-day Cs concentration of 0.008 g/L, or in the worst case for the 700°C heat treatment, the Cs 7-day Cs concentration is 0.175 g/L. For additional comparison, a borosilicate glass formulation, R7T7, which contains 1.42 wt% Cs and a total alkali content of 13.26 wt%, has a Cs leach rate of 0.16 g/m^2•day.[4]

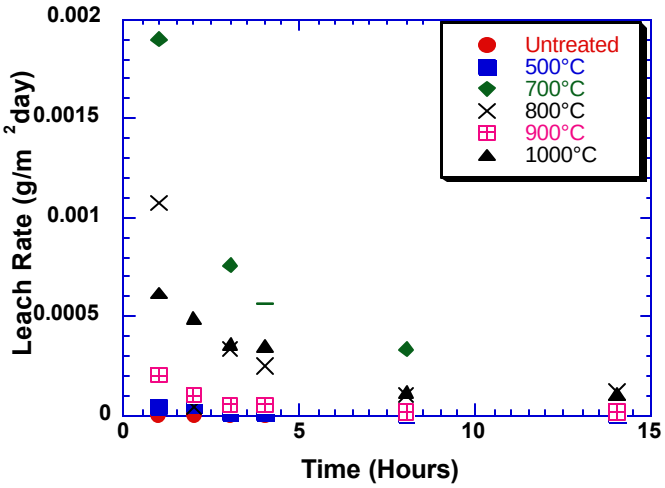

Figure 1. PCT aqueous leach rate for waste forms synthesized by simply heat-treating CST IE-911 over a range of temperatures. Before heat treatment, IE-911 was treated with NaOH and exchanged for 12 wt% Cs.

The aqueous durability behavior, as measured by the PCT test, for both as-received and Na-exchanged IE-911 loaded to 5 wt% and 12 wt% Cs did not show any significant differences. Leach rates measured using the MCC-1 test were even lower than those measured by the PCT test, as expected.

The durability tests show that heat-treated IE-911 with no additives can result in a chemically durable waste form. Thermogravimetric and differential thermal analysis of Cs-exchanged and Na,Cs-exchanged IE-911 was performed to determine decomposition and crystallization temperatures. This analysis revealed that all molecular water is desorbed by 400°C, and hydroxyl groups are removed near 800°C. Therefore, the risk of radiolytic hydrogen production during short- or long-term storage is eliminated by heat- treating the ion exchanger to temperatures above 800°C. The volume reduction of a pellet heat-treated to 900°C is 40%. [2]

2. Structure/Property Relationship Studies

A. Phase Selection of Thermally Converted CST

Phase stability and crystal chemistry studies for compositions related to the exchanger are vital to predicting long- and short-term performance of waste forms. Cs-loaded IE-911 contains six or more constituents including Cs_2O, Na_2O, SiO_2, TiO_2, binder, and proprietary components. While the phase relationships between some of the binary and ternary components of the CST are

available in the literature, the phase selection and durabilities of more complex compositions that represent the loaded exchanger are unknown.

X-ray diffraction of heat-treated IE-911 powders shows that the single phase metastable ion exchanger structure is destroyed above 500°C, then at higher temperatures, stable multiphase crystalline mixtures precipitate. Positive identification by XRD had already been achieved for the sodium titanate phase, $Na_2Ti_6O_{13}$. This structure is a layered structure. While there are known isomorphs for potassium and rubidium substitutions on this structure, cesium substitution had not been documented. The structure of the pure cesium analog, $Cs_2\ Ti_6O_{13}$, has a different structure than the sodium, potassium, or rubidium forms. To determine whether small amounts of cesium could reside in the $Na_2\ Ti_6O_{13}$ structure, a solid substitution series of $(Na, Cs)_2\ Ti_6O_{13}$ was synthesized, and the lattice parameters were measured by XRD. This study surprisingly revealed that there is no measurable substitution of cesium for sodium on the $Na_2\ Ti_6O_{13}$ lattice, eliminating the possibility that small amounts of cesium could reside in this phase in heat-treated IE-911.

^{133}Cs magic angle spinning nuclear magnetic resonance measurements were performed to reveal the local environment around the Cs atom. Figure 2 shows the NMR spectra for NaOH-treated, Cs-exchanged IE-911 heat-treated over a range of temperatures. It can be seen from the spectra that the Cs environment in the as-received exchanger is destroyed above 500°C. Broadening of the peak at 500°C indicates that the material is becoming amorphous. At 700°C a new Cs-containing phase forms, and by 800°C the peak representing the original Cs-environment is completely gone. The single, sharp high- temperature peak indicates that the Cs is in only one crystalline environment.

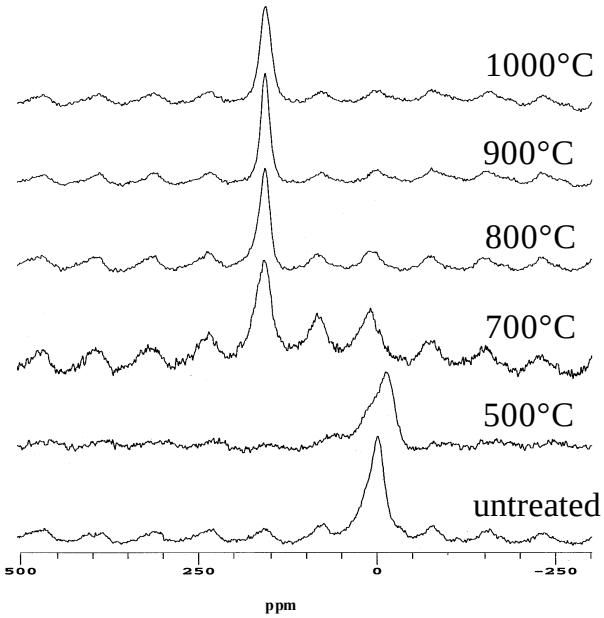

Figure 2. ^{133}Cs MAS NMR spectra for NaOH-treated, 12 wt% Cs-exchanged IE-911 heat-treated over a range of temperatures.

Transmission electron microscopy (TEM) study was further performed to evaluate the phase selection of thermally converted CST. Figure 3 shows a micrograph of a thin section of 12 wt% cesium-exchanged IE-911. Among these were Cs, X1, Si oxide, Na, Ti oxide, Na, Ti, X2 oxide, and very minor Na, Cs, Ti, Si, X1 oxide, where X1 and X2 are proprietary components of the ion exchanger.

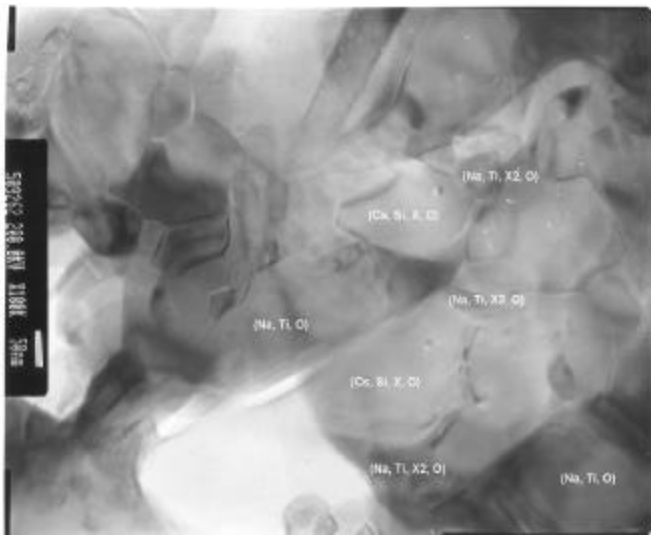

Figure 3. TEM micrograph of a thin section of IE-911 that was treated in NaOH, exchanged with 12 wt% Cs, then heat-treated to 900°C. Energy dispersive spectroscopy of individual grains revealed the approximate compositions of the phases in this proposed waste form.

TEM revealed that the majority of the Cs is contained in a Cs, X1, Si oxide. This phase was successfully synthesized using solid-state reaction, sol gel, and hydrothermal reactions. The stoichiometry of the phase is $Cs_2X1Si_3O_9$. While a similar phase is reported in the literature, the crystal structure of this compound is unknown, and the powder XRD data are incomplete. We attempted to grow single crystals of this compound; however, due to the refractory nature of the proprietary component, no suitable crystals have been synthesized to date. Rietveld refinement of X-ray powder diffraction data showed that $Cs_2X1Si_3O_9$ has a hexagonal structure (space group P63/m) with lattice parameters a=7.2303(2) Å, c=10.2682(4) Å. [5] The simulated crystal structure based on the atomic positions of the isomorph and the lattice parameters of $Cs_2X1Si_3O_9$ is shown in Figure 4. It consists of silica tetrahedra and X1 octahedra that form three-membered and six-membered rings. The largest free aperture of the rings is approximately 2.2x2.6 Å, which is smaller than a Cs atom (~3.5 Å). Therefore, the Cs in this phase will be immobile. Removal of Cs from the structure will require the cleavage of the strong, covalent Si-O and X1-O bonds. This structural feature in part explains the high resistance to leaching of Cs in thermally converted IE-911 that is exposed to aqueous solutions.

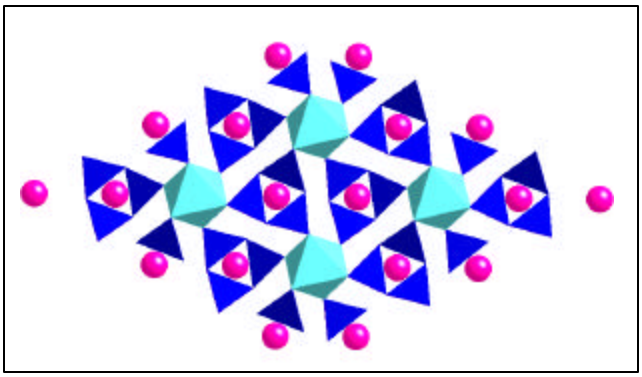

Figure 4. View of $Cs_2X1Si_3O_9$ structure down the [001] directions. This is the major Cs-containing phase in thermally converted (900°C) IE-911.

A second new phase discovered in TEM (Na, Ti, X2, oxide) has a structure similar to $NaX2O_3$. To determine the extent of titanium substitution in the mixed phase, a series of compounds with up to 20% titanium substituted for X2 were synthesized using a sol gel technique. A systematic shift of the lattice parameter as a function of titanium substitution clearly could be observed. Comparison of the heat-treated IE-911 with the synthesized compounds revealed that the phase in IE-911 has 15% titanium substitution on the lattice. The structure of the new compound is related to a perovskite; however, the distribution of the cations in the structure is unknown.

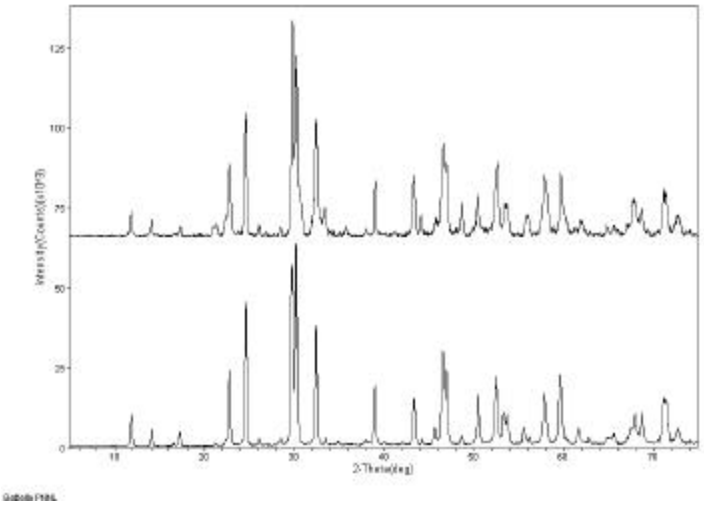

Figure 5. Comparison of the experimental XRD pattern of mixed-phase Cs-exchanged IE-911 heat-treated to 900°C (upper pattern) with a simulated pattern that is a compilation of the X-Ray patterns from synthesized compounds $Na_2Ti_6O_{13}$, $Cs_2X1Si_3O_9$, and $Na(Ti, X2)O_3$ (lower pattern). The excellent match between the two patterns suggests that these compounds represent the major phases in the waste form.

With the discovery of the two new oxide phases in heat-treated CST, the phase identification is nearly complete. Figure 5 shows the XRD pattern of Cs-exchanged heat-treated IE-911 compared with a simulated X-ray pattern, which is a combination of the patterns of the three

phases identified in this program, $Na_2Ti_6O_{13}$, $Cs_2X1Si_3O_9$, and $Na(Ti, X2)O_3$. It can be seen that all of the major peaks have been identified. Several very small peaks that appear in the thermally converted IE-911 pattern are not present in the simulated pattern. The intensity of these peaks decreases significantly with longer heat treatment at 900°C or with heat treatment to 1000°C, indicating that this phase is metastable.

B. Stable Phases in Cs_2O-TiO_2-SiO_2 System

Phase equilibria studies in the model system, Cs_2O-TiO_2-SiO_2, are being performed to identify the stable compounds in this system and to determine their compositional regions of stability.[6-11] The phase relationships for compositions related to the ion exchanger will provide information necessary for setting optimal composition and temperature regimes for processing of the final waste form and will elucidate the effects of minor compositional variations. Our current understanding of the phase equilibria is illustrated in Figure 6.

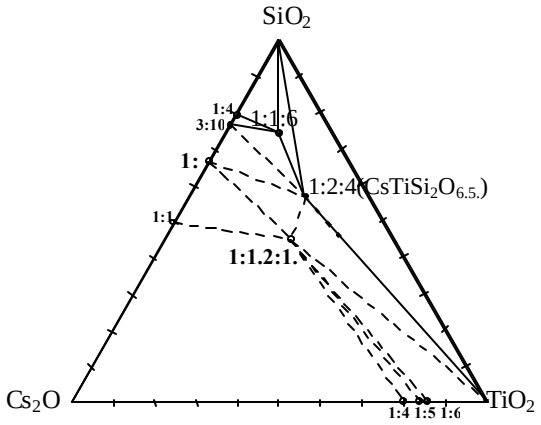

Figure 6. Phase equilibrium diagram for Cs_2O-TiO_2-SiO_2

Two new high-temperature, durable, high-Ti crystalline zeolitic phases of $CsTiSi_2O_{6.5}$ and $Cs_2TiSi_6O_{15}$ were synthesized and characterized.[6-11] $CsTiSi_2O_{6.5}$ has a crystal structure isomorphous to the mineral pollucite, $CsAlSi_2O_6$, with Ti^+ replacing Al^+. The structure of $Cs_2TiSi_6O_{15}$ is unique, with titanium octahedra and silicon tetrahedra forming an open framework structure with the Cs residing in large cavities. The largest covalently bonded ring opening to the Cs cavities in both compounds are smaller than a Cs ion, revealing that the Cs ion has minimal mobility in the structure. Therefore, both compounds have exceptional resistance to leaching.

Single-crystal growth experiments have produced a new tetragonal structure that is similar to cubic pollucite (1:2:4 Cs_2O-TiO_2-SiO_2) but with extended TiO_2 solubility. In addition, a new compound with stoichiometry 1:1.2:1.7 Cs_2O-TiO_2-SiO_2 has been identified. Determination of the crystal structure of these new compounds is in progress.

A complete solid solution series between$CsTiSi_2O_{6.5}$ and $CsAlSi_2O_6$ has been synthesized. This is interesting because the substitution of aluminum by titanium is charge-balanced by the incorporation of additional oxygen ions, converting four coordinated aluminum to five

coordinated titanium. Thus, the rather unusual ionic substitution $Al^{3+} = Ti^{4+} + ½ O^{2-}$ is occurring. Lattice parameters versus Ti contents vary in a complex way, especially for Ti-rich compositions (Figure 7). Rietveld analysis of our synchrotron XRD data reveal that the structure of pollucite ($CsAlSi_2O_6$) is slightly tetragonal (space group $I4_1/a$; c/a ≈ 1.0014) whereas those for all other compositions are cubic (space group $Ia3d$). Therefore, substitution of Ti^{4+} for Al^{3+} in pollucite can lead to stabilization of the cubic structure at room temperature. On cooling, however, the Ti-substituted pollucites undergo a cubic-to-tetragonal phase transition, as revealed by subambient powder X-ray diffraction (Figure 8). This transition is displacive in character and probably involves both delocalization of Cs+ ions and distortion of Si/Al/Ti framework.[12] Moreover, the critical temperature of the transition appears to decrease linearly with increasing Ti content.

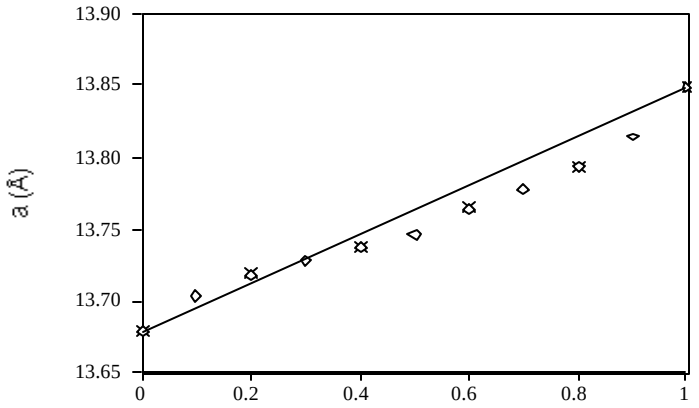

Figure 7. Variation of cell parameter *a* for $CsTi_xAl_{1-x}Si_2O_{6+0.5x}$ pollucites as a function of composition. For ease of comparison, the cell parameters for the tetragonal pollucite $CsAlSi_2O_6$ are represented by $V^{1/3}$ here. Cross = synchrotron X-ray data; Diamond = conventional X-ray data. Errors are smaller than the size of symbols.

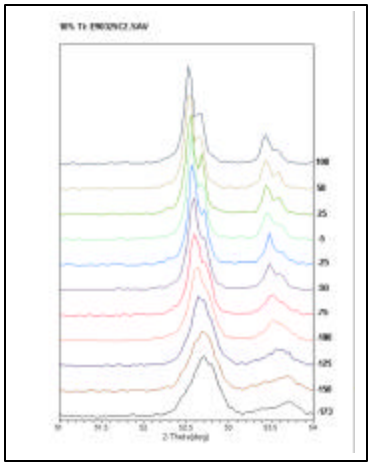

Figure 8**.** Change of XRD pattern for $CsAl_{0.9}Ti_{0.1}SiO_{6.05}$ as a function of temperature.

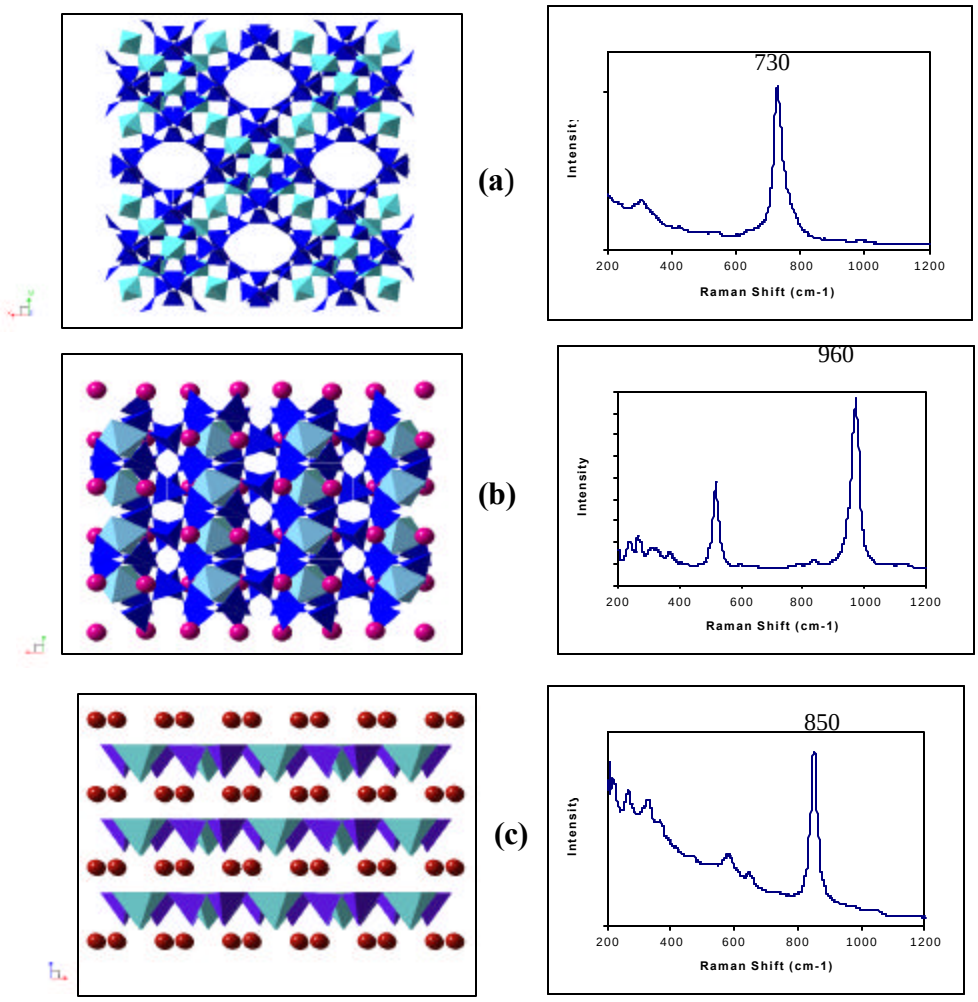

Figure 9. Crystal structure and Raman spectra of (a) ETS-10, (b) $Cs_2TiSi_6O_{15}$, (c) $Ba_2TiSi_2O_8$

Raman spectroscopy studies were performed to determine correlations between Raman shifts with silicon and titanium structural units, especially titanium coordination in silicotitanate compounds.[11] We found that unique Raman shifts were generated for isolated and connected (corner or edge-shared) Ti polyhedra. For example, the compound ETS-10 that contains corner-shared octahedral Ti chains shows Raman features at 730 cm^{-1}, whereas isolated Ti octahedra in the compound $Cs_2TiSi_6O_{15}$ give a unique Raman shift at 960 cm^{-1} (see Figure 9, a and b). For silicotitanates that contain TiO_5 in a square pyramidal configuration with one short Ti-O bond, such as $Ba_2TiSi_2O_8$, a strong band at 850 cm^{-1} due to Ti=O stretch will be observed in Raman spectra (see Figure 9, c).

C. Metastable Phases in Cs_2O-TiO_2-SiO_2 System

Researchers at SNL are studying the metastable phase development in the component systems that represent the Cs-loaded ion exchanger. This work complements the stable phase development studies at PNNL and allows for a complete understanding of the phase development from the metastable ion exchanger to the stable ceramic waste form. Hydrothermal Cs_2O-TiO_2-SiO_2 ternary phase searches have produced two novel phases, which we have

designated SNL-A and SNL-B.[13-16] The stability regions of these phases (5 days at 170°C) as a function of Cs_2O:TiO_2:SiO_2 precursor ratio (and pH) are plotted on the ternary diagram in Figure 10. These experiments show a distinct relationship between SNL-B and SNL-A. At 170°C, SNL-B is formed in a mixture with SNL-A. With increased time at temperature, only SNL-A is formed. For example, at 120°C for 5–20 days, only SNL-B is formed, while at 120°C for 28 days, only SNL-A is formed. Also shown on the ternary plot is the stability region for TiO_2 and pharmacosiderite (a known microporous Cs_2O-TiO_2-SiO_2 ion exchanger).

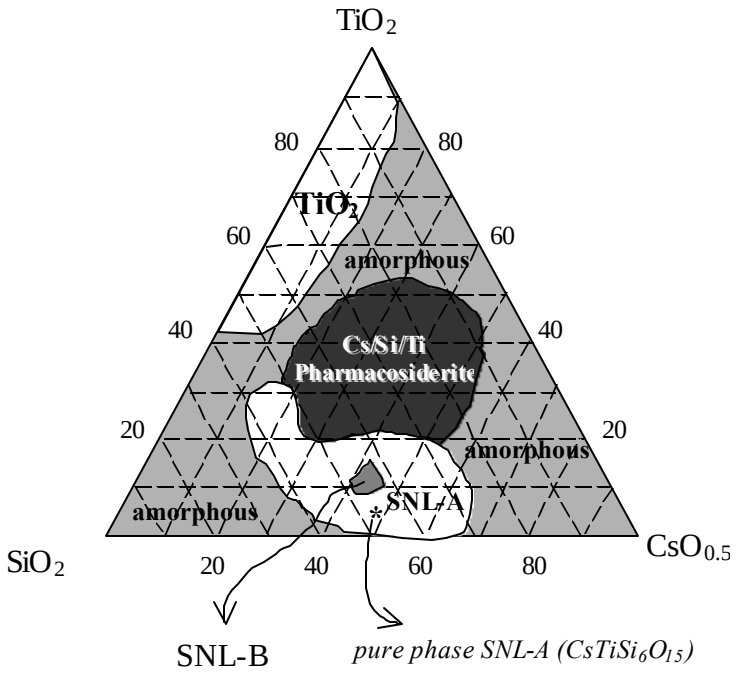

Figure 10. Stability of hydrothermally synthesized Cs_2O-TiO_2-SiO_2 ternary phases at 170°C

SNL-A is a condensed phase with a formula $Cs_2TiSi_6O_{15}$, polymorphic to the phase synthesized at PNNL by solid-state techniques. The structure of SNL-A has been solved by structure modeling (using Density Functional Theory Calculations) and Rietveld refinement. SNL-A crystallizes in the monoclinic (Cc) space group with unit cell parameters; a = 12.998 (2) Å, b = 7.5014 (3) Å, c = 15.156 (3) Å, β = 105.80 (3)°. The framework of SNL-A consists of silicon tetrahedra and titanium octahedra that condense in 3-, 5-, 6-, 7- and 8-rings. The Cs ions are located in cages created by the rings. PCT leach tests performed on this phase for 10 days showed <0.2% Cs loss from the original 30% by weight Cs composition; effectively no Cs was lost due to leaching.

SNL-B is a microporous ion exchanger with a chemical formula $Cs_3TiSi_3O_{9.5}\cdot 3H_2O$. This molecular sieve exhibits high selectivity for divalent cations. Solid state ^{133}Cs and ^{29}Si MAS-NMR (magic angle spinning nuclear magnetic resonance) and CP (cross polarization) MAS NMR of SNL-A and SNL-B reveal that both phases are structurally complex with multiple silicon and Cs coordination sites. All silicon atoms in both phases are in tetrahedral coordination. The CP-MAS NMR experiments show there is internal water in SNL-B and none in SNL-A. This is confirmed by thermogravimetry experiments.

In situ TEM-monitored electron irradiation studies of SNL-A and SNL-B were also carried out (in collaboration with Dr. Rodney Ewing at the University of Michigan) to determine the stability of these new phases in radioactive environments. The irradiation-induced transformation of microporous crystalline SNL-B to amorphous material is observed by fading Bragg-diffraction spots in the electron diffraction pattern. The irradiation dose needed for amorphization of SNL-B is inversely dependent on temperature. This corresponds to heat-accelerated Cs and/or water loss, and finally a thermally induced phase change at 500°C (which is also observed by differential thermal analysis). This amorphization behavior is typical of other zeolite materials studied by Dr. Ewing. The condensed phase SNL-A, on the other hand, is very irradiation-resistant. It does not undergo any irradiation damage with very high dose rates.

D. New Sr-Selective Microporous Ion Exchanger

In the course of Na_2O-TiO_2 hydrothermal phase searches, researchers at SNL discovered a new inorganic molecular sieve, Na/Nb/M/O (M=Ti and Zr), with extreme selectivity for divalent elements, especially Sr and RCRA metals, as observed in Table 1 (Phase I is a Ti-niobate phase, Phase II is a Zr-niobate phase).[17-19] They are chemically and mechanically stable, have high selectivity for divalent radwaste cations and RCRA metals, are regenerable (by back ion exchange) and thermally converted to a refractory and unreactive perovskite-based ceramic.

This ion exchanger shows high selectivity over the entire pH scale, with maximum K_ds of 10^6 in basic solutions to 10^3 in acid solutions. Distribution coefficients of phase I with each cation of Na concentration as a competing ion is shown in Figure 11.

Table 1. Distribution Coefficient of a Variety of Exchange Metals on Niobate Phases at pH =7

metal	**radius in pm (6-coordinate)**	**Phase I (K_d, ml/g)**	**Phase II (K_d, ml/g)**
Pb^{2+}	133	66,497	22,022
Cr^{3+}	94	> 99,800	> 99,800
Co^{2+}	89	> 99,800	> 99,800
Ni^{2+}	83	> 99,800	> 99,800
Zn^{2+}	88	> 99,800	> 99,800
Cd^{2+}	109	> 99,800	> 99,800
Cs^{+}	181	150	169
K^{+}	152	95	153
Li^{+}	90	8	35
Ba^{2+}	149	> 99,800	> 99,800
Sr^{2+}	132	> 99,800	> 99,800
Ca^{2+}	114	2300	2657
Mg^{2+}	86	226	458

At lower Na concentrations (< 0.1 M Na), the K_d values approach 10^6 ml/g, which is the value obtained for approximately 0.1 ppm Sr remaining in solution; the detection limit of the Sr analytical technique (AAS). As [Na] increases, the K_ds decrease to approximately 500 ml/g.

Figure 12 shows a plot of distribution coefficient of Sr on Phase I as a function of pH with 0 M Na, 0.01 M Na and 0.1 M Na as a competing ion.

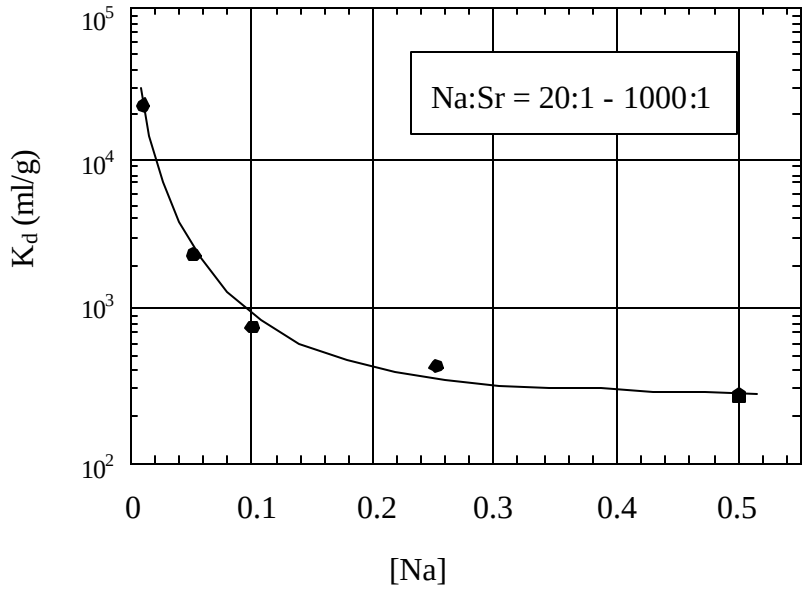

Figure 11. Selectivity of Strontium (50 ppm) as a Function of [$NaNO_3$] in Solution on Phase I.

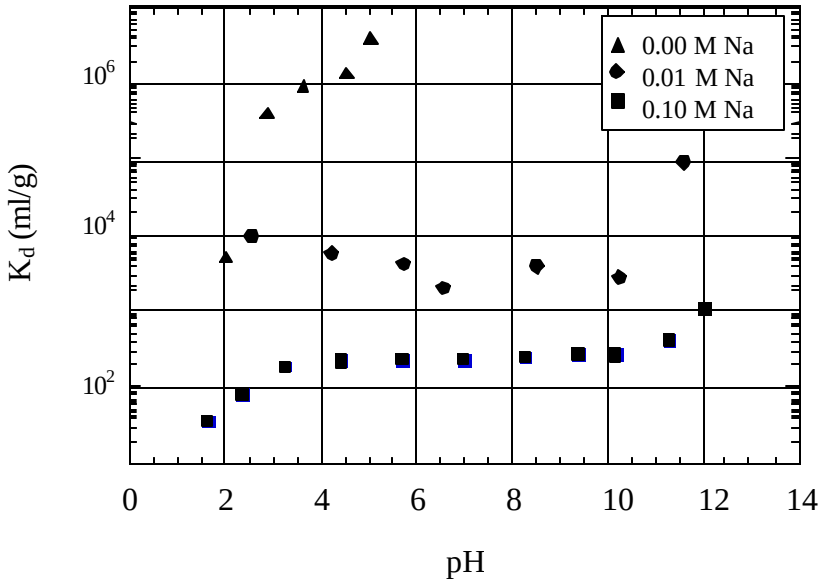

Figure 12. Selectivity of Sr (50 ppm) as a function of pH on Phase II.

The purpose of using Na as a competing ion for these studies is twofold: 1) to suppress the Sr selectivity so that K_d values may be obtained; and 2) addition of NaOH is necessary for the higher pH experiments, so a consistent concentration of sodium (combination of $NaNO_3$ and NaOH) is added to all the experiments to keep the solution matrices as similar as possible. In general, there is an increase in Sr selectivity with increasing basicity. However, above pH = 12,

Sr uptake is decreased. This correlates with an increase in $Sr(OH)^+$ concentration in solution; above pH = 12.8, $Sr(OH)^+$ becomes the sole Sr species in solution.[17-21] This result suggests either 1) supporting evidence is provided for the ion exchanger's selectivity for divalent cations; or 2) the pore size limits uptake of $Sr(OH)^+$. The selectivity experiments with 0 M Na were carried out only in the acidic range because at pH > 6, all Sr is removed from solution. With lower concentrations of Na (0.01, 0), the selectivity for Sr remains surprisingly high (>10^4ml/g), which is several orders of magnitude higher than other Sr selective phases. [17] On the other hand, high concentrations of Na inhibits Sr selectivity considerably. However; to compare this effect directly to the performance of other Sr selective ion exchangers such as layered titanates and silicotitanates, experiments using very high hydroxyl concentrations need to be executed. Below pH = 1.5, the niobate ion exchanger undergoes decomposition, and selectivity decreases. Decreased ion adsorption is typical of inorganic ion exchangers in acidic solutions. The anionic framework preferentially takes up H^+ from the acidic solution over the larger metal cations. Conversely, in highly basic solutions where H^+ concentration is low, the ion exchanger adsorbs metal cations. Finally, maximum Sr-loading of Phase I was accomplished by twice-repeated contact and agitation of the ion exchangers with 1M $Sr(NO_3)_2$ solutions. The final Na:Sr ratio of the maximum exchanged phases is 4:1.

3. Thermodynamic Studies Using High-Temperature Reaction Calorimetry

A. Energetics of CST Ion Exchangers

Using hydrothermal methods, two series of microporous silicotitanates were synthesized at SNL: 1) $(Na_{1-x}Cs_x)_3Ti_4Si_3O_{13}(OH)\cdot xH_2O$ (x = 4-5) phases with a cubic structure of $P\bar{4}3m$ (analogues of the mineral pharmacosiderite) and 2) $(Na_xCs_{1-x})_3Ti_4Si_2O_{13}(OH)\cdot xH_2O$ (x = 4-5) phases with a tetragonal structure of $P4_2/mcm$.[13-22] The enthalpies of drop solution in molten $2PbO\cdot B_2O_3$ at 974K were measured at UC Davis by high-temperature reaction calorimetry. Combining the measured data with the published enthalpies for the constituent oxides, the enthalpies of formation for the silicotitanate phases were determined for the first time.[18] The enthalpies of formation for the cubic phases become more exothermic as Cs/(Na+Cs) increases (Figure 13a), whereas those for the tetragonal phases become less exothermic (Figure 13b). This result indicates that the Cs uptake in the cubic phases is thermodynamically favorable, whereas that in the tetragonal phases is thermodynamically unfavorable and kinetically driven. In addition, the cubic phases appear to be more stable than the corresponding tetragonal phases with the same Cs/Na ratio. We attribute these disparities in the energetic behavior for the two series to their differences in both local bonding configuration and degree of hydration.

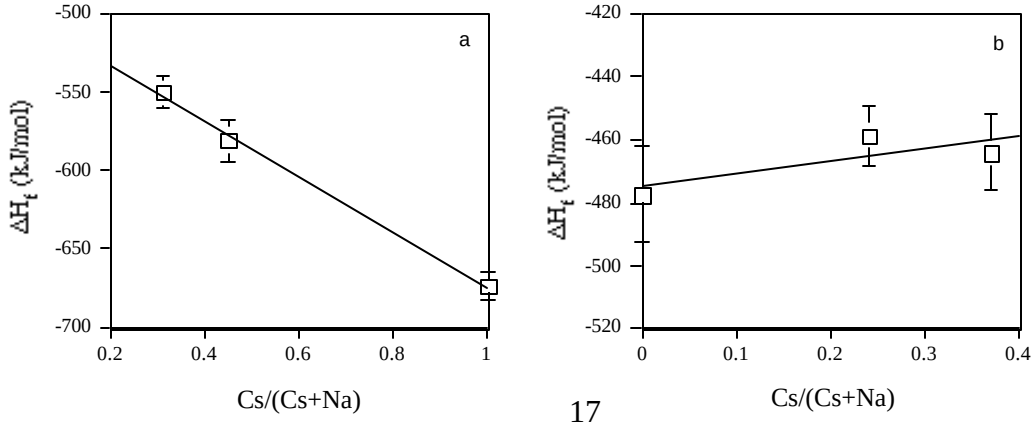

Figure 13. Enthalpies of Formation from Oxides of (a) the Cubic Phases and (b) the Tetragonal Phases as a Function of Composition.

B. Energetics of Ti-Substituted Pollucites

A complete solid solution series between $CsAlSi_2O_6$ and $CsTiSi_2O_{6.5}$ was synthesized using the sol-gel method at PNNL. The structures of the Ti-substituted pollucites are analogous to that of cubic pollucite ($CsAlSi_2O_6$), as determined by Rietveld analysis of powder synchrotron XRD data. The standard molar enthalpies of formation from the oxides for Ti-substituted pollucites were determined at UC Davis by drop solution calorimetry.[23,24] As Ti^{4+} substitutes for Al^{3+} in pollucites, the enthalpies of formation become less exothermic, suggesting a destabilizing effect of the charge-coupled substitution, $Ti^{4+} + 1/2O^{2-} \rightarrow Al^{3+}$, on the pollucite structure. Moreover, the enthalpic variation shows an exothermic mixing within the composition range from $CsTi_{0.3}Al_{0.7}Si_2O_{6.15}$ to $CsTiSi_2O_{6.5}$ (Figure 14). This non-ideal mixing behavior is consistent with the trend seen in variation of lattice parameters (Figure 7), and we interpret it to be a result of the short-range order associated with the framework cations Al^{3+}, Si^{4+}, and Ti^{4+} in the structures.

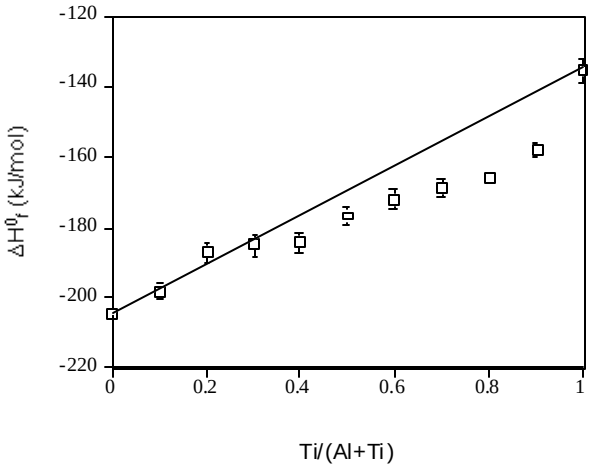

Figure 14. Enthalpies of Formation of Substituted Pollucites $CsTi_xAl_{1-x}Si_2O_{6+0.5x}$ from Constituent Oxides as a Function of Composition

C. Energetics of Ti-substituted Niobate Perovskites

Using the sol-gel method, researchers at PNNL have recently synthesized a series of Ti-substituted niobate perovskites with the compositions $NaTi_xNb_{1-x}O_{3-0.5x}$, $0 \le x \le 0.3$, in which a portion of Nb^{5+} is replaced by Ti^{4+} and the charge is balanced by the creation of O^{2-} vacancies. Preliminary XRD experiments reveal that the structure of Ti-substituted perovskite systematically varies with increasing Ti content, inducing a series of compositionally driven transitions that are analogous to those for $NaNbO_3$ at elevated temperatures. The standard molar enthalpies of formation from the oxides for Ti-substituted perovskites were determined at UC Davis by drop solution calorimetry. As Ti^{4+} substitutes for Nb^{5+}, the enthalpies of formation

become less exothermic (Figure 15). This behavior suggests that the Ti-Nb substitution slightly destabilize the structure (with respect to the constituent oxides), presumably due to the occurrence of O^{2-} vacancies in the structure.

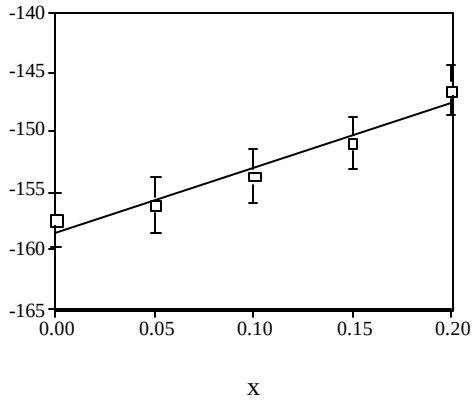

Figure 15. Enthalpies of Formation of the $NaTi_xNb_{1-x}O_{3-0.5x}$ Perovskites from Constituent Oxides as a Function of Composition

4. Radiation Stability Studies

Radiation stability studies by gamma irradiation in the PNNL ^{60}Co source as well as by in situ TEM electron beam with the collaboration of Professor Rodney Ewing at the University of Michigan) were completed. For the gamma irradiation studies, both Cs loaded IE-911 and the Cs-containing phase $Cs_2XSi_3O_9$ were exposed to gamma irradiation at a dose rate of approximately $9x10^5$ Rad/hr at various temperatures (50 to 200ºC). The total absorbed dose was $5.2x10^{10}$ Rad. XRD analysis shown in Figures 16 and 17 indicates there is no radiation-induced damage or amorphization. These results suggest that $Cs_2XSi_3O_9$ and IE-911 have good radiation stability and are suitable for waste form applications. In contrast, preliminary results from in situ TEM electron irradiation show amorphization after an electron fluence of $1.1x10^{22}$ e/cm^2. Correlations between the absorbed dose received by electron irradiation and those received by gamma irradiation is the subject of ongoing research.

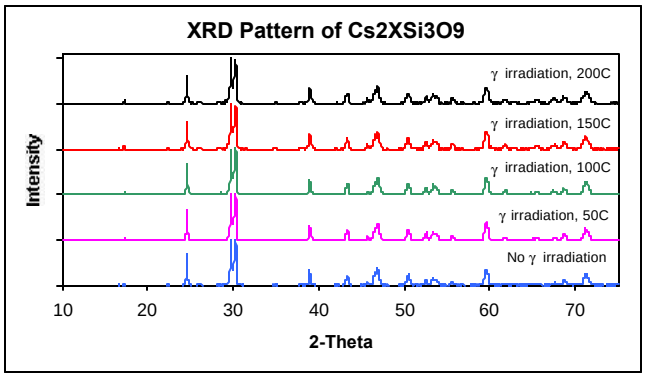

Figure 16. Comparison of X-ray diffraction patterns for $Cs_2XSi_3O_9$ before and after exposure to gamma irradiation at various temperatures.

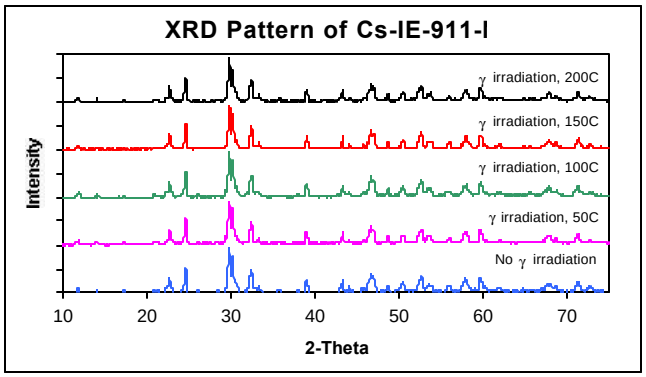

Figure 17. Comparison of X-ray diffraction patterns for the ion exchanger IE-911 loaded with 12 wt% Cs before and after exposure to gamma irradiation at various temperatures.

5. Summary

In summary, we have shown that a very durable waste form can be achieved by a simple heat treatment of the Cs-loaded ion exchanger with no additives. Direct thermal conversion reduces the total volume of waste generated from the ion exchanger by 40% and dramatically simplifies processing. Heat treatment of the ion exchanger coarsens fines, reducing inhalation risk, and removes water, eliminating radiolytic hydrogen production. The IE-911 CST ion-exchanger is compositionally complex. Transmission electron microscopy, XRD, and synthesis studies have revealed that the major phases in CST are $Na_2Ti_6O_{13}$, $Cs_2X1Si_3O_9$, and $Na(Ti,X2)O_3$. The network structure of the Cs-containing phases precludes facile migration of the Cs ion, resulting in extremely high aqueous durability. Metastable phase-development studies have revealed two new low temperature Cs/Si/Ti phases and a novel class of niobate-based molecular sieves (Na/Nb/M/O, M = transition metals), which show exceptionally high selectivity for divalent cations. These niobate materials have shown orders of magnitude better selectivity for Sr^{2+} under acid conditions than any other material. In addition, the thermodynamic stabilities of metastable and stable compounds have been determined by solution-drop calorimetry. This combined information on phase selection as a function of composition, chemical durablity, and thermodynamic stability can be used to determine processing windows and to predict long- and short-term stability of thermally converted CST ion exchangers.

Relevance, Impact and Technology Transfer

The scientific knowledge gained through this program can be applied to the critical DOE/EM problem of Cs and Sr separation and sequestration at several DOE sites including SRS and Hanford. The DOE and researchers at the Savannah River Site are currently evaluating the best method for Cs separation from tank waste at SRS. Ion exchange of Cs using the CST, specifically IE-911, is one of two processes being considered for Cs separation. Studies at SRS and ORNL indicated that irreversible Cs desorption occurred with small temperature fluctuations (55-80°C). Currently, PNNL and SNL are part of a team that is investigating the cause of the irreversible desorption. Fundamental aspects of our EMSP research, such as the relationships between Raman spectra and structural features in silicotitanates, are being used to determine if

Cs desorption is a result of structural degradation of IE-911. In addition, the catalog of possible phases and their structures that was developed in the EMSP program is vital information to identify phases that may form if some degradation of IE-911 occurs. Because conventional techniques often offer incomplete structural information, the interpretation of more advanced structural probes such as those developed in this work are also critical tools. In addition, thermodynamic stability studies for Na, and Cs exchanged CSTs completed on the EMSP program provide insight to the driving force for Cs desorption.

This new EM-funded, mission directed, joint interaction between the researchers from the EMSP program and the end users of the ion exchanger at Savannah River is a direct product of the EMSP program. The data collected on this program will contribute to meeting DOE milestones and will provide SRS with critical information to assess damage that could occur from temperature excursions that could occur during a process upset. This work addresses a near-term EM need at SRS and a potential longer term need at Hanford.

Project Productivity

The project accomplished the proposed goals on schedule. In addition, work on the program lead to new discoveries not anticipated in the original proposal. Of particular importance was the discovery of a new ion exchanger material that is selective for divalent cations.

Personnel Supported/Associated with the Research Effort

Dr. M. Lou Balmer, PNNL
Dr. Yali Su, PNNL
Dr. Tina Nenoff, SNL
Dr. May Nyman, SNL
Prof. Alexandra Navrotsky, UC Davis
Dr. Hongwu Xu, UC Davis
Dr. Robert Roth, NIST/Viper Group
Prof. Rod Ewing, Univ. of Michigan
Dr. Lumin Wang, Univ. of Michigan
Binxi Gu, Univ. of Michigan
Dr. Nancy Hess, PNNL
Dr. LiQiong Wang, PNNL
Dr. Akilesh Tripathi, SUNY, Stony Brook
Dr. John Parise, SUNY, Stony Brook
Prof. William Harrison, Univ. of Aberdeen
Dr. Ian Grey, CSIRO
Dr. Robert Maxwell, LLNL

Publications

Yali Su, Mari Lou Balmer, and Bruce Bunker, “Raman Spectroscopic Studies of Silicotitanates,” J. Phys. Chem. B, 2000, 104, 8160-8169.

Xu, H., Navrotsky, A.; Nyman, M. D.; Nenoff, T. M. Thermochemistry of microporous silicotitanate phases in the Na2O-Cs2O-SiO2-TiO2-H2O System. *Journal Materials Research*, **2000**, *15*(3), 815.

Nyman, M.D., Gu, B.X., Wang, L.M., Ewing, R.C., Nenoff, T.M. 2000. "Synthesis and Characterization of a New Microporous Cesium Silicotitanate (SNL-B) Molecular Sieve, " *Journal of Microporous and Mesoporous Materials*, 2000, *34*, 301.

M.L. Balmer , Y. Su, H. Xu , E.R. Bitten, D.E. McCready, and A. Navrotsky "Synthesis, Structure Determination, and Aqueous Durability of $Cs_2ZrSi_3O_9$." Journal of the American Ceramic Society, 2000, in press.

Nyman, M., Bonhomme, F., Teter, D. M., Maxwell, R. S., Gu, B. X., Wang, L. M., Ewing, R. C., Nenoff T. M., " Integrated Experimental and Computational Methods for Structure Determination and Characterization of a New, Highly Stable Cesium Silicotitanate Phase, $Cs_2TiSi_6O_{15}$ (SNL-A)." *Chem. Mater*., 2000, in press.

Nyman, M. D., Harrison, W. T. A., Maxwell, R. S., Tripathi, A., Parise, J.; Nenoff, T. M. "Sandia Octahedral Molecular Sieves (SOMS): A new class of molecular sieve materials." *Nature*, 2000, submitted.

Xu, H., A. Navrotsky, M.L. Balmer, Y. Su, E. Bitten. 2000. "Energetics of substituted pollucites along the $CsAlSi_2O_6$-$CsTiSi_2O_{6.5}$ join: A high-temperature calorimetric study," submitted to *Journal of the American Ceramic Society*.

Conference Proceedings

Xu, H., A. Navrotsky, M.L. Balmer, Y. Su, E. Bitten, T.M. Nenoff, and M.D. Nyman. 1999. "Thermochemistry of substituted pollucites along the $CsAlSi_2O_6$-$CsTiSi_2O_{6.5}$ join," EOS (American Geophysical Union 1999 Fall Meeting), Vol. 80. No. 46, F1115.

Nyman, M. and T. M. Nenoff. 1999. "Synthesis, Characterization and Ion Exchange of New Na/Nb/M4+/OH2O (M = Ti, Zr) Phases", *in Proceedings from the Metal Separation Technologies Beyond 2000,* Hawaii.

Nenoff, T.M., M. Nyman, A. Navrotsky, H. Xu, Y. Su, and M.L. Balmer. 1999. "Synthesis, Characterization and Ion Exchange of Novel Sodium Niobate Phases, " in *Proceedings from ACS Symposium on First Accomplishments of Environmental Management Science Program*. New Orleans, August 1999.

Su, Y. , M.L. Balmer, and B.C. Bunker. 1997. "Evaluation of Cesium Silicotitanates as an Alternative Waste Form," in *Scientific Basis for Nuclear Waste Management XX*. Vol. 465, Edited by W.J. Gray and U.R. Triay, Materials Research Society, pp 457-464, Warrendale, PA. Su, Y., M.L. Balmer, L. Wang, B.C. Bunker, M.D. Nyman, T. Nenoff, and A. Navrotsky. 1998.

Su, Y., M.L. Balmer, L. Wang, B.C. Bunker, M.D. Nyman, T. Nenoff, and A. Navrotsky. 1998. "Evaluation of thermally converted silicotitanate waste forms", in *Scientific Basis for Nuclear*

Waste Management XXII Vol. 556, D. J. Wronkiewicz and J. H. Lee eds., p77-84, Materials Research Society, Warrendale, PA.

Nyman, M.D., T.M. Nenoff, Y. Su, M.L. Balmer, A. Navrotsky, and H. Xu. 1998. "CSTs: Stability and Use as Alternative Waste Forms," in *Scientific Basis for Nuclear Waste Management XXII* Vol. 556, D. J. Wronkiewicz and J. H. Lee eds., p71-76, Materials Research Society, Warrendale, PA.

Invited Presentations

H. Xu, A. Navrotsky, M.L. Balmer, Y. Su, E.R. Bitten, T.M. Nenoff, and M.D. Nyman, Synthesis, crystal chemistry, and energetics of substituted pollucites along the $CsAlSi_2O_6$-$CsTiSi_2O_{6.5}$ join. American Geophysical Union 2000 Spring meeting, Washington, DC, May 30 - June 3, 2000.

T.M. Nenoff and M.D. Nyman, "Novel Niobate based Molecular Sieves with Selectivity for divalent cations, "16th Annual Canadian Catalysis Society Meeting, Banff, AB, Canada; May 2000

M.L. Balmer, "New Silicotitanate Waste Forms: Development and Characterization," Plenary Lecture, EMSP National Workshop, Atlanta, GA, April 24-28, 2000.

Presentations

T. M. Nenoff, M. D. Nyman; A. Tripathi; J. Parise; R. Ewing, "OMS, A New Classes of Na/Nb/X/O microporous and perovskite phases" Fall 2000 National MRS Meeting, Boston, MA; December 2000.

M. D. Nyman; T. M. Nenoff; F. Bonhomme, D. M. Teter; R. S. Maxwell; H. Xu; A. Navrotsky, "Synthesis, Characterization and calorimetric studies of A2TiSi6O15 (A = Na, K, Cs)," Fall 2000 National ACS Meeting, Washington, DC; August 2000.

Yali Su, M. Lou Balmer, Eric Bitten and Dave McCready, Hongwu Xu, Alexandra Navrotsky, Binxi Gu, Luming Wang, and Rodney Ewing , "Synthesis, Structure Determination, and Aqueous Durability of $Cs_2ZrSi_3O_9$ and $Cs_2TiSi_6O_{15}$" American Ceramic Society 102nd Annual Meeting in St. Louis, Missouri, April 30-May3, 2000.

T.M. Nenoff, M. D. Nyman, and R. Ewing, "Na/Nb/X/O and Cs/Si/Ti Selective microporous and perovskite phases:Characterization and novel synthesis methods," EMSP annual review Meeting, Atlanta, GA; May 2000.

Y. Su, M.L. Balmer, E. Bitten, H. Xu, A. Navrotsky, M.D. Nyman, T.M. Nenoff, and, R.S. Roth, "Development and Characterization of Ceramic Waste Forms from Cs-Loaded Crystalline Silicotitanates, ", MRS 1999 Fall meeting, Boston, Nov 29-Dec. 3, 1999.

H. Xu, A. Navrotsky, M.L. Balmer, Y. Su, E. Bitten, T.M. Nenoff, and M.D. Nyman, "Thermochemistry of substituted pollucites along the $CsAlSi_2O_6$-$CsTiSi_2O_{6.5}$ join," American Geophysical Union 1999 Fall meeting, San Francisco, California, December 13-17, 1999.

H. Xu, A. Navrotsky, M.D. Nyman, T.M. Nenoff, M.L. Balmer, and Y. Su, Thermochemistry of microporous silicotitanate phases in the Na_2O-Cs_2O-SiO_2-TiO_2-H_2O system. 101th Annual Meeting of the American Ceramic Society, Indianapolis, IN, April 25-28, 1999.

T. M. Nenoff, M. D. Nyman, R. Ewing, "Na/Nb/X/O microporous and perovskite phases: Characterization and novel synthesis methods." Spring 2000 National ACS Meeting, San Francisco, CA; March 2000.

"Phase Selection, Crystal Structure, and Durability of Cs-Silicotitanates," Y. Su, M.L. Balmer, E. Bitten, A. Navrotsky, H. Xu, T. Nenoff and M. Nyman, 218th American Chemical Society Meeting National Meeting in New Orleans, LA , August 22-26, 1999.

Y. Su and M. L. Balmer, " Raman Spectroscopic Studies of Silicotitanates", American Ceramic Society Conference in Indianapolis IN, April 25, 1999.

"Evaluation of Thermally Converted Silicotitanate Waste Forms," M.L. Balmer, Y. Su, A. Navrotsky, H. Xu, T. Nenoff and M. Nyman, 215th Annual Meeting of the American Chemical Society, Dallas, TX, March 29-April 2, 1998.

Interactions

As detailed in the section on *Relevance, Impact and Technology Transfer*, principal investigators at PNNL and SNL are supporting DOE on Cs separation using IE-911. This interaction was established at the EMSP workshop, 2000 in Atlanta.

Transitions

Currently, PNNL and SNL are part of a team that is investigating the cause of the irreversible desorption of Cs from IE-911 during small temperature fluctuations.

The enabling research is the phase selection, thermal stability, and crystal chemistry work. Contacts that have been established and are making use of our research include Bill Wilmarth from SRS, Paul Taylor from ORNL, Rich Braun from UOP, and Dennis Wester from PNNL.

Patents

U. S. Patent submitted: Nenoff, T. M.; Nyman, M. D.; Cesium Silicotitanates for Ion Exchange and Waste Storage, 2000.

U. S. Patent submitted: Nenoff, T. M.; Nyman, M. D.; Novel Niobate based molecular sieves, 2000.

Future Work

The experimental work on this EMSP program is complete. A small amount of funding that remains is being used to complete several manuscripts.

A renewal proposal was funded for this work. The new work will focus on optimizing the properties and developing structure property relationships for the new class of metal niobate ion exchangers discovered in this EMSP program.

Literature Cited

1. Su, Y. , M.L. Balmer, and B.C. Bunker. 1997. "Evaluation of Cesium Silicotitanates as an Alternative Waste Form," in *Scientific Basis for Nuclear Waste Management XX*. Vol. 465, Edited by W.J. Gray and U.R. Triay, Materials Research Society, pp 457-464, Warrendale, PA.
2. Su, Y., M.L. Balmer, L. Wang, B.C. Bunker, M.D. Nyman, T. Nenoff, and A. Navrotsky. 1998. "Evaluation of thermally converted silicotitanate waste forms", in *Scientific Basis for Nuclear Waste Management* XXII Vol. 556, D. J. Wronkiewicz and J. H. Lee eds., p77-84, Materials Research Society, Warrendale, PA.
3. Ferrara, D.M., M.K. Andrews, J.R. Harbour, T.L. Fellinger, D.T. Herman, K.M. Marshall, and P.J. Workman. 1997. "Vitrification of Ion Exchange Material," WSRC-TR-97-00320, Sept. 30, 1997.
4. Nogues, J.L., E.Y. Vernaz, and N. Jacquet-Francillon. 1984. in *The Scientific Basis for Nuclear Waste Management*, Vol. 44, Carol M. Jantzen, John A. Stone, and Rodney C. Ewing, eds., Materials Research Society, Warrendale, PA.
5. Balmer, M.L., Y. Su, H. Xu, E. Bitten, D. McCready, and A. Navrotsky. 1999. "Synthesis, Structure Determination, and Aqueous Durability of $Cs_2ZrSi_3O_9$, " in press, *J. Am. Ceram. Soc.*
6. Balmer, M. L., Y. Su, I.E. Grey, A. Santoro, R.S. Roth, Q. Huang, N. Hess and B.C. Bunker. 1996. "The structure and properties of two new silicotitanate zeolites", in *Scientific Basis for Nuclear Waste Management XX* Vol. 465, W.J. Gray and I.R. Triay eds., p. 449, Materials Research Society, Warrendale, PA.
7. McCready, M. L., M.L. Balmer, and K.D. Keefer. 1997. "Experimental and Calculated X-ray Powder Diffraction Data for Cesium Titanium Silicate, $Cs_2Ti_2Si_4O_{13}$: A New Zeolite," *Powder Diffraction*, 12 (1), pp. 40-46.
8. Balmer, M.L., Q. Huang, A. Santoro, and R. Roth. 1997. "Neutron Powder Diffraction Study of the Crystal Structure of $CsTiSi_2O_{6.5}$," *J. Sol. State Chem*., 130, pp. 97-102.
9. Grey, I.E., R.S. Roth, and M.L. Balmer. 1997. "The Crystal Structure of $Cs_2TiSi_6O_{15}$," *J. of Sol. State Chem*., Vol. 131, pp. 38-42.
10. Balmer, M.L., B.C. Bunker, L.Q. Wang, C.H.F. Peden, and Y. Su. 1997. "Solid State ^{29}Si MAS NMR of Titanosilicates," *J. Phys. Chem*., Vol. 101, No. 45, pp. 9170-9179.
11. Su, Y., M.L. Balmer, and B.C. Bunker. 2000. "Raman Spectroscopic Studies of Silicotitanates, " *J. Phys. Chem. B*, 2000, 104, 8160-8169.
12. Palmer, D.C., Dove, M.T., Ibberson, R.M., and Powell, B.M. 1997 "Structural behavior, crystal chemistry, and phase transitions in substituted leucite: High-resolution neutron powder diffraction studies." Am. Minearl., 82, 16.

13. Nyman, M.D., T.M. Nenoff, Y. Su, M.L. Balmer, A. Navrotsky, and H. Xu. 1998. “CSTs: Stability and Use as Alternative Waste Forms," in *Scientific Basis for Nuclear Waste Management XXII* Vol. 556, D. J. Wronkiewicz and J. H. Lee eds., p71-76, Materials Research Society, Warrendale, PA.
14. Nyman, M.D., Gu, B.X., Wang, L.M., Ewing, R.C., Nenoff, T.M. 2000. “Synthesis and Characterization of a New Microporous Cesium Silicotitanate (SNL-B) Molecular Sieve, ” *Journal of Microporous and Mesoporous Materials*, 2000, *34*, 301.
15. Nyman, M., Bonhomme, F., Teter, D. M., Maxwell, R. S., Gu, B. X., Wang, L. M., Ewing, R. C., Nenoff T. M., " Integrated Experimental and Computational Methods for Structure Determination and Characterization of a New, Highly Stable Cesium Silicotitanate Phase, $Cs_2TiSi_6O_{15}$ (SNL-A)." *Chem. Mater*., 2000, in press.
16. U. S. Patent submitted: Nenoff, T. M.; Nyman, M. D.; Cesium Silicotitanates for Ion Exchange and Waste Storage, 2000.
17. Nyman, M. D., Harrison, W. T. A., Maxwell, R. S., Tripathi, A., Parise, J.; Nenoff, T. M. "Sandia Octahedral Molecular Sieves (SOMS): A new class of molecular sieve materials." *Nature*, 2000, submitted.
18. U. S. Patent submitted: Nenoff, T. M.; Nyman, M. D.; Novel Niobate based molecular sieves, 2000.
19. Nyman, M. and T. M. Nenoff. 1999. “Synthesis, Characterization and Ion Exchange of New Na/Nb/M4+/OH2O (M = Ti, Zr) Phases”, *in Proceedings from the Metal Separation Technologies Beyond 2000*, Hawaii.
20. Nenoff, T.M., M. Nyman, A. Navrotsky, H. Xu, Y. Su, and M.L. Balmer. 1999. “Synthesis, Characterization and Ion Exchange of Novel Sodium Niobate Phases, ” in *Proceedings from ACS Symposium on First Accomplishments of Environmental Management Science Program*. New Orleans, August 1999.
21. Nenoff, T.M., J. E. Miller, S. G. Thoma, and D. E. Trudell. 1996. " Highly Selective Inorganic Crystalline Ion Exchange Material for Sr^{2+} in Acidic Solutions," *Environ. Sci. Technol.* 30, 3630.
22. Xu, H., Navrotsky, A.; Nyman, M. D.; Nenoff, T. M. Thermochemistry of microporous silicotitanate phases in the Na2O-Cs2O-SiO2-TiO2-H2O System. *Journal Materials Research*, **2000**, *15*(3), 815.
23. Xu, H., A. Navrotsky, M.L. Balmer, Y. Su, E. Bitten, T.M. Nenoff, and M.D. Nyman. 1999. "Thermochemistry of substituted pollucites along the $CsAlSi_2O_6$-$CsTiSi_2O_{6.5}$ join," EOS (American Geophysical Union 1999 Fall Meeting), Vol. 80. No. 46, F1115.
24. Xu, H., A. Navrotsky, M.L. Balmer, Y. Su, E. Bitten. 2000. "Energetics of substituted pollucites along the $CsAlSi_2O_6$-$CsTiSi_2O_{6.5}$ join: A high-temperature calorimetric study," submitted to *Journal of the American Ceramic Society*.

Appendix A: Submitted Papers

Journal of the American Ceramic Society Ms. #188537

Energetics of Substituted Pollucites Along the $CsAlSi_2O_6$-$CsTiSi_2O_{6.5}$ Join: A High-Temperature Calorimetric Study

Hongwu Xu* and Alexandra Navrotsky*

Thermochemistry Facility, Department of Chemical Engineering and

Materials Science, University of California at Davis, Davis, CA 95616, USA

M. Lou Balmer,* Yali Su,* and Eric R. Bitten

Pacific Northwest National Laboratory, P.O. Box 999,

MSIN K8-93, Battelle Blvd., Richland, WA 99352, USA

*Member, American Ceramic Society

Submitted on May 22, 2000

Revised on September 20, 2000

Abstract

Enthalpies of drop solution for a suite of substituted pollucites with the compositions $CsTi_xAl_{1-x}Si_2O_{6+0.5x}$, $0 \leq x \leq 1$, which were synthesized using the sol-gel method, have been measured in molten $2PbO \cdot B_2O_3$ at 701 °C. As Ti^{4+} substitutes for Al^{3+}, the enthalpies of drop solution become less endothermic and show exothermic heats of mixing within the composition range from x = 0.3 to 1. This non-ideal mixing behavior is consistent with the trend seen in variation of lattice parameters, and we interpret it to be a result of the short-range order associated with the framework cations Al^{3+}, Si^{4+}, and Ti^{4+} in the structure. Using enthalpies of drop solution of SiO_2, Al_2O_3, TiO_2 and Cs_2O, standard molar enthalpies of formation of these phases from their constituent oxides and from the elements were derived for the first time.

I. Introduction

Pollucite, $CsAlSi_2O_6$, has a three-dimensional framework structure composed of corner-sharing $(Si,Al)O_4$ tetrahedra with Cs^+ cations occupying its cavities.[1,2] This material is of considerable interest because it has relatively high resistance to alteration under hydrothermal conditions and thus can potentially be used as a solid host for radioactive Cs immobilization.[3-6] Pollucite is also interesting for its unique thermal expansion behavior and hence for its use as a component in high-temperature glass-ceramic materials.[7-9] In addition, natural pollucite, which commonly contains the analcime ($NaAlSi_2O_6 \cdot H_2O$) component and mainly occurs in rare-element granitic pegmatites, is the primary industrial source of Cs and is of petrogenetic interest as an indicator of the advanced stage in pegmatitic magma fractionation.[10,11]

Pollucite is the Cs-exchanged form of leucite ($KAlSi_2O_6$). Leucite undergoes two successive displacive phase transitions, $I4_1/a \rightarrow I4_1/acd$ at ~667 °C and $I4_1/acd \rightarrow Ia3d$ at ~687 °C, on heating.[12-17] Replacing K^+ with the larger Cs^+ in the structural cavities mimics the effect of increasing temperature, that is, propping open the tetrahedral framework and thus increasing the stability field of the cubic phase.[15,17] As a result, pollucite was found to have substantially lowered transition temperatures (*e.g.*, 97 °C)[17] or even be cubic at room temperature.[4,7-9,18-20]

Ionic substitutions in the leucite structure can occur not only in the cavity site but over the framework cation positions as well.[17] A series of recent studies by Balmer and co-workers have demonstrated that Ti^{4+} can substitute for Al^{3+} in pollucite and the charge is balanced by the incorporation of extra O^{2-} anions into the structure.[21-25] This peculiar mechanism produces a series of substituted pollucites with the general formula $CsTi_xAl_{1-x}Si_2O_{6+0.5x}$, $0 \leq x \leq 1$.[25]

Interest in the Ti-substituted pollucites has largely been stimulated by their potential uses for the storage of radioactive Cs.[21-25] Recent studies[26,27] show that some silicotitanate ion exchangers have high selectivities for Cs^+ over Na^+, and thus they could be used for the separation of ^{137}Cs from radioactive aqueous wastes with high Na^+ concentrations (such as those at Hanford, Washington). The Cs-loaded

silicotitanate microporous phases can then be heat-treated *in situ* to produce a thermally stable and chemically durable ceramic waste form.[27-29] This waste disposal strategy may reduce cost compared with other plans and minimize the risk of environmental contamination.[27-29] As a possible host for Cs in the proposed waste form, the Ti-substituted pollucite, $CsTiSi_2O_{6.5}$, was found to have Cs leach rates comparable to those of aluminosilicate pollucite.[3,21]

To evaluate the feasibility of Ti-substituted pollucites as waste forms for Cs, a thorough understanding of their energetics and its relation to their crystal chemistry is essential. In this study, we synthesized a series of pollucites along the $CsAlSi_2O_6$- $CsTiSi_2O_{6.5}$ join using the sol-gel method. Their enthalpies of mixing and heats of formation from constituent oxides were determined by high-temperature drop-solution calorimetry with lead borate as the solvent. Trends in the enthalpies as a function of composition allow analysis of the crystal chemistry of this series from an energetic perspective.

II. Experimental Methods

(1) Sample Synthesis

Eleven substituted pollucites with the composition $CsTi_xAl_{1-x}Si_2O_{6+0.5x}$, x = 0.0 - 1.0 with an interval of 0.1, were synthesized via a sol-gel processing route (Balmer et al. in preparation). First, an amorphous, homogeneous precursor for each composition was prepared using tetraethyl orthosilicate (TEOS), aluminum tri-sec-butoxide (ATSB), titanium isopropoxide (TIP), and cesium hydroxide. The alkoxides (TEOS, ATSB and TIP) were mixed in stoichiometric ratio in a glove box under argon atmosphere and then a mixture of CsOH, water, and ethanol was added. The resulting hydrolyzed precursor was stirred for a minimum of 15 h and then dried in air at room temperature. Second, approximately 0.5 g of the obtained precursor was annealed at a temperature ranging from 825 to 1200 °C, depending on the composition, for about 15 h (except for the $CsTiSi_2O_{6.5}$ phase, which was heat-treated for 2 h). The resulting product is a white, monophasic crystalline material, as revealed by X-ray

diffraction (see below). Electron microprobe analysis of two samples (x = 0.1 and 0.7) confirm that their compositions agree well with the nominal values and that the samples are homogeneous.

(2) Powder X-ray Diffraction

Powder X-ray diffraction (XRD) experiments were performed with both synchrotron and conventional X-ray radiation. Synchrotron XRD was conducted for the $CsTi_xAl_{1-x}Si_2O_{6+0.5x}$ samples with x = 0, 0.2, 0.4, 0.6, 0.8 and 1, using a linear position-sensitive detector (PSD) at beam line X7A[30] of the National Synchrotron Light Source (NSLS), Brookhaven National Laboratory (BNL). The wavelength used was 0.7076 Å, as calibrated using a CeO_2 standard. The powder samples were sealed in silica-glass capillaries of 0.2 mm diameter, and the capillaries were fully rotated during data collection. Data were collected from 4 to 50° 2θ in step scan mode using steps of 0.25° with counting times of 10 s (4-15.5°), 20 s (15.5-27°), 40 s (27-38.5°) and 80 s (38.5-50°) per step.

The Rietveld method[31] was used to analyze the synchrotron data with the General Structure Analysis System (GSAS) program of Larson and Von Dreele.[32] The starting atomic parameters were taken from the study of pollucite by Newnham.[18] Peak shapes were fitted with a pseudo-Voigt function,[33,34] and backgrounds were modeled with a radial distribution function. The final value of the agreement index R_{wp}, after the atomic positions and temperature factors were refined, ranges from 2.8% to 3.7%. Details of the full structural refinements are presented in a separate paper (Xu et al., in preparation).

Conventional XRD was carried out for all the eleven samples, using a Phillips X'Pert MPD/PW3050 diffractometer with Cu$K\alpha$ radiation and a solid-state scintillation detector. To determine the unit-cell parameters, sample powders for each composition were mixed with a silicon standard (NIST SRM 640b) in a 3:1 weight ratio, and the mixture was mounted in a front-loading, shallow-cavity holder. Data were collected from 10° to 130° 2θ in step scan mode using steps of 0.025° with a counting time of 2 s. Peak positions were calibrated using Si as the standard, and unit-cell parameters were refined with the program MDI Jade 5.1.

(3) High-Temperature Drop Solution Calorimetry

High-temperature calorimetric measurements were performed using a Tian-Calvet microcalorimeter operating at ~701 °C with molten lead borate ($2PbO \cdot B_2O_3$) as the solvent. The equipment and experimental procedure have been described in detail by Navrotsky.[35] A sample pellet weighing ~5 mg was dropped from room temperature into the solvent in the hot calorimeter. The enthalpy measured includes the energy associated with heating the sample from room temperature to 701 °C plus the enthalpy of solution of the sample. The calorimeter was calibrated against the known heat contents of corundum pellets weighing ~5 mg. Between six to ten sample pellets were dropped for each composition. To ensure there is no surface water, which would have a significant endothermic effect, present in the samples, all the samples were dried at 130 °C overnight immediately before the calorimetric experiments.

III. Results and Discussion

(1) Structural Behavior

Rietveld analyses of our synchrotron XRD data show that all the $CsTi_xAl_{1-x}Si_2O_{6+0.5x}$ phases adopt the framework topology of leucite. However, the structure of pollucite ($CsAlSi_2O_6$) appears to be tetragonal (space group $I4_1/a$),[17] though its cell dimensions along the **a**- and **c**-axes are only slightly different (c/a □ 1.0014), whereas those for all other compositions are cubic (space group $Ia3d$). The framework of pollucite consists of corner-sharing $(Si,Al)O_4$ tetrahedra that are arranged in four-, six-, and eight-membered rings (Fig. 1A). In this structure, there are three kinds of symmetrically distinct tetrahedral sites over which Si and Al are disordered.[17] Cs ions occupy the cavity sites in 12-fold coordination, which are interconnected by channels through the six-membered rings along [111] (Fig. 1A). Substitution of Ti^{4+} for Al^{3+} in the structure increases the symmetry from tetragonal to cubic and thus decreases the number of symmetrically distinct framework sites from three to one. To compensate the charge imbalance between Al^{3+} and Ti^{4+}, this substitution is accompanied by incorporation of extra O^{2-}

anions into the structure (Fig. 1B).[21-25] A previous neutron diffraction study of the end member $CsTiSi_2O_{6.5}$ reveals that the extra oxygens are located in two sets of general sites with small fractions of occupancy (*i.e.*, 0.060 and 0.023).[23] Further, X-ray absorption spectroscopy (XAS) analysis of this compound favors a five-fold coordination of Ti^{4+},[22] implying that these extra oxygens are bonded to Ti^{4+} (forming a titanyl TiO_5 group), rather than to Si^{4+}. In addition, because of the presence of excess oxygens, the average coordination of Cs^+ is increased to 13-fold,[21,23] as compared to 12-fold in pollucite. This charge-coupled substitution and the induced local structural change are thus quite unusual.

Unit cell parameters of the $CsTi_xAl_{1-x}Si_2O_{6+0.5x}$ phases are listed in Table I. The cell parameters obtained by Rietveld analysis of the synchrotron XRD data and those by least-squares fitting of the conventional XRD data are in good agreement. The compositions were calculated from the starting stoichiometry. The trend of increasing cell parameter a and cell volume V with increasing x is consistent with the replacement of Al^{3+} by the larger Ti^{4+} and the incorporation of extra O^{2-} into the structure. However, the variation of a or V vs. x is not linear; it shows a negative deviation from the ideal linearity when x = 0.3 to 1 (Fig. 2). We attribute this behavior to varying degrees of short-range order associated with the framework cations Si^{4+}, Al^{3+}, and Ti^{4+}, across the series (see discussion below).

In addition, no obvious discontinuity in the dependence of cell volume V on x is seen when the structure changes from tetragonal for x = 0 to cubic for x $\square$ 0.1 (Fig. 2). This behavior suggests that the tetragonal pollucite is structurally very similar to the cubic phase (x $\square$ 0.1), as is also reflected by the closeness of its cell parameters a and c (Table I).

(2) Enthalpies of Mixing

The heats of drop solution ($\square H_{ds}$) of the $CsTi_xAl_{1-x}Si_2O_{6+0.5x}$ phases are presented in Table II and Figure 3A. $\square H_{ds}$ becomes less endothermic with increasing Ti content. Further, variation of $\square H_{ds}$ exhibits deviations from a straight line, which would represent the $\square H_{ds}$ for a mechanical mixture between the two end-members (ideal mixing). This trend is consistent with that displayed by the variation of lattice

parameters as a function of composition, as is reflected by the approximately linear relation between ΔH_{ds} and cell volume *V* (Fig. 3B).

Enthalpies of mixing (ΔH_{mix}) for the solid solutions are determined by subtracting the ΔH_{ds} value measured for each phase from that of the mechanical mixture of the two end members at the same composition (Fig. 4). The ΔH_{mix} values for phases from x = 0 to 0.3 are zero within the errors of our measurements. In contrast, solid solutions within the compositional range, $0.3 < x < 1$, clearly show exothermic enthalpies of mixing, suggesting that these phases are energetically more stable than their corresponding mechanical mixtures.

The enthalpic variations induced by the substitution, $Ti^{4+} + 1/2\ O^{2-} \rightarrow Al^{3+}$, must result from the corresponding changes in structure. Within the $0 \leq x \leq 0.3$ regime, the cell volume V and thus the enthalpy ΔH_{ds} show an approximately linear variation with x. As described earlier, the pollucite end member, unlike other compositions, adopts a tetragonal structure with slightly different *a* and *c*. Above ~97 °C,[17] however, it transforms displacively to the cubic structure. Since the calorimetric temperature of ~701 °C places pollucite well into the field of its cubic structure, the measured ΔH_{ds} value actually includes the enthalpy associated with the transition (ΔH_{tran}). Nevertheless, as this transition only involves very slight tilting of $(Si,Al)O_4$ tetrahedra,[17] ΔH_{tran} is presumably small and it very likely falls within the uncertainties of our measurements.

The exothermic mixing behavior for compositions from x = 0.3 to 1 (Fig. 4), is correlated with their negative deviations in cell volume from the ideal volume of mixing (Fig. 2). In other framework aluminosilicates such as feldspars[36], the energetic properties vary with the state of Si-Al order. Analogously, the increased stability for pollucite phases within the $0.3 < x < 1$ regime with respect to their mechanical mixtures is probably due to increased degrees of ordering associated with their framework cations (Si^{4+}, Al^{3+}, and Ti^{4+}). Moreover, a decrease in cell volume with increasing extent of ordering is consistent with the trends observed in many other materials.[37] Although the cubic pollucite structure has one type of crystallographically distinct site for framework cations, which precludes any long-range Si/Al/Ti order in the Ti-substituted pollucites, it is still very likely that these cations are ordered on a

local scale. It is also likely, as discussed above, that the locations of Ti^{4+} and of excess O^{2-} are strongly correlated.

(3) Framework Cation Ordering

In framework aluminosilicates, the tetrahedrally coordinated Si and Al cations tend to distribute themselves in ways that minimize the number of Al-O-Al linkages (the so-called "Al avoidance principle" or "Loewenstein's rule").[38,39] The crystal-chemical explanation for this phenomenon is that O in the Al-O-Al linkage (net oxygen charge = -0.5)[40] is more underbonded than O in Si-O-Al (net charge = -0.25). As a result, the Al-O-Al configuration is energetically unfavorable relative to Al-O-Si. A previous ^{29}Si and ^{27}Al NMR study of a pollucite sample, which is the Cs-exchanged product of natural leucite crystals, reveals not only the absence of Al-O-Al linkages but also a slight degree of short-range order associated with the next-nearest neighbors (*e.g.*, in favor of Si-O-Si-O-Al linkages relative to Al-O-Si-O-Al).[41] This result suggests that Al and Si in this ion-exchanged pollucite have a strong tendency to be ordered on various local scales.

With Ti^{4+} substituting for Al^{3+} in pollucite, additional O^{2-} is incorporated into the structure to maintain charge neutrality. As a result, the substituted Ti^{4+} becomes five-fold coordinated by oxygen,[22] as compared with four-fold coordination for Al^{3+}. To achieve a pentacoordinate geometry for every Ti^{4+}, however, the O must be shared by two [TiO_5] pyramids via edge-sharing.[23] Therefore, Ti-O-Ti (and possibly Al-O-Ti) linkages can occur in the Ti-substituted pollucites, though these configurations are considered slightly unfavorable based on Loewenstein's rule (net oxygen charge = -0.4 for Ti-O-Ti and -0.45 for Al-O-Ti).[42] In other words, some degree of Si/Al/Ti disorder may exist in these structures. Furthermore, the disordering degree probably increases with increasing Ti content. Although no NMR data are available for intermediate phases, a previous ^{29}Si NMR measurement of the end-member $CsTiSi_2O_{6.5}$ shows that two of 13 T-O-T (T = Si or Ti) linkages in a unit-cell could be Ti-O-Ti.[24] This bond configuration also satisfies the geometrical constraint for the paired [TiO_5] pyramids in the structure.[23,24]

It should be stressed that the above considerations of framework cation ordering are purely on a crystal-chemical basis. In reality, however, the state of order (equilibrium or non-equilibrium) for a sample also depends on its formation conditions and thermal history. This is why the crystal-chemical considerations, which suggest a decrease in the degree of Si/Al/Ti order with increasing substitution of Ti^{4+} for Al^{3+}, cannot fully account for the non-linear enthalpy variation with Ti content (Fig. 3A). Because the gels with different compositions, from which the pollucite samples were crystallized, have different crystallization temperatures and melting points (*e.g.*, $CsAlSi_2O_6$ has a crystallization temperature of 1026 °C,[43] and $CsTiSi_2O_{6.5}$ has a melting point of 980 °C[23]), it is not possible to synthesize all these samples at the same temperature. The somewhat irregular variation in the annealing temperature used with Ti content (Balmer et al. in preparation) probably causes a corresponding complex variation in the degree of Si/Al/Ti order. This behavior may thus result in the complex trends in both the energetic and the structural variation as a function of composition (Fig. 2 and 3A). To further establish the relation between the state of Si/Al/Ti order of Ti-substituted pollucites and their energetic behavior, ^{29}Si NMR and Ti XAS measurements for these samples are currently being performed.

(4) Enthalpies of Formation

Using previously determined enthalpies of drop solution of Cs_2O, Al_2O_3, TiO_2, and SiO_2 (Table III), and our measured calorimetric data for the $CsTi_xAl_{1-x}Si_2O_{6+0.5x}$ phases (Table II), we calculated their standard molar enthalpies of formation from the constituent oxides ($\Delta H_{f,ox}^0$) via the following thermochemical cycle:

$$(1/2)Cs_2O\ (s, 25\ °C) \rightarrow (1/2)Cs_2O\ (soln, 701\ °C) \quad (1)$$

$$xTiO_2\ (s, 25\ °C) \rightarrow xTiO_2\ (soln, 701\ °C) \quad (2)$$

$$(1/2 - x/2)Al_2O_3\ (s, 25\ °C) \rightarrow (1/2 - x/2)Al_2O_3\ (soln, 701\ °C) \quad (3)$$

$$2SiO_2\ (s, 25\ °C) \rightarrow 2SiO_2\ (soln, 701\ °C) \quad (4)$$

$$(1/2)Cs_2O\ (soln, 701\ °C) + xTiO_2\ (soln, 701\ °C) + (1/2 - x/2)Al_2O_3\ (soln,$$

701 °C) + $2SiO_2$ (soln, 701 °C) → $CsTi_xAl_{1-x}Si_2O_{6+0.5x}$ (s, 25 °C) (5)

(1/2)Cs_2O (s, 25 °C) + $xTiO_2$ (s, 25 °C)+ (1/2 – x/2)Al_2O_3 (s, 25 °C)

+ $2SiO_2$ (s, 25 °C) → $CsTi_xAl_{1-x}Si_2O_{6+0.5x}$ (s, 25 °C) (6)

from which the enthalpies of formation of the $CsTi_xAl_{1-x}Si_2O_{6+0.5x}$ phases are computed as follows: $\Delta H_{f,ox}^0 = \Delta H_1 + \Delta H_2 + \Delta H_3 + \Delta H_4 + \Delta H_5$.

Similarly, the enthalpies of formation of these phases from the elements ($\Delta H_{f,el}^0$) can be derived from their $\Delta H_{f,ox}^0$ values and the $\Delta H_{f,el}^0$ values of the constituent oxides (Table III) by using an appropriate reaction cycle. The enthalpies of formation thus obtained are presented in Table II. The only previously reported enthalpies of formation in this system are on pollucite, measured by HF solution calorimetry.[48] However, the sample used was a natural pollucite $[(Cs_{0.650}Na_{0.185}Rb_{0.028})(AlSi_2)(O_{5.863}OH_{0.137})\cdot 0.19H_2O]$ containing the analcime component, and its $\Delta H_{f,ox}^0$ and $\Delta H_{f,el}^0$ were determined to be –209.50 ± 2.38 and –3098.52 ± 3.63 kJ/mol, respectively.[48] These values are more negative than the corresponding $\Delta H_{f,ox}^0$ and $\Delta H_{f,el}^0$ values, -204.3 ± 1.8 and –3036.6 ± 2.8 kJ/mol, measured by us for the pure end-member.

As shown in Figure 5, $\Delta H_{f,ox}^0$ becomes less exothermic as substitution of Ti^{4+} for Al^{3+} increases. This behavior suggests a destabilizing effect of the charge-coupled substitution, $Ti^{4+} + 1/2\ O^{2-} \rightarrow Al^{3+}$, on the pollucite structure. One of the factors responsible for this destabilization is the larger cation size difference between Si^{4+} and Ti^{4+} compared to that between Si^{4+} and Al^{3+}, resulting in increased strain energy as the Ti content increases. In addition, the incorporation of extra O^{2-} anions in the Ti-substituted pollucites, which rarely occurs in other framework silicates, might also destabilize these structures. Moreover, as evident in Figure 5, the $\Delta H_{f,ox}^0$ values exhibit significant deviations from the straight line that represents ideal mixing, and we attribute this behavior to the varying degrees of Si/Al/Ti order across the series, as described earlier.

Although the thermodynamic stability of the substituted pollucites relative to their constituent oxides decreases with increasing $Ti^{4+} + 1/2\ O^{2-} \rightarrow Al^{3+}$ substitution, the stability of this series with respect

to the aqueous species appears not to vary significantly with composition. Specifically, the two end-members $CsAlSi_2O_6$ and $CsTiSi_2O_{6.5}$ were found to have comparable low rates of Cs leaching.[3,21] This behavior is probably related to their similar small sizes of cages in which Cs ions reside, rendering the low mobility of Cs^+ in both structures.[21] The Cs release under aqueous conditions might be also controlled by kinetic factors. As demonstrated in our recent studies on two series of microporous titanosilicate phases,[44] kinetic factors do seem to play significant roles in the uptake of Cs in titanosilicate structures. To further reveal the relations among structure, energetics, kinetics, and physical properties of the pollucite series, however, more detailed investigations would be needed.

IV. Conclusions

A complete series of pollucite solid solutions has been synthesized between the compositions $CsAlSi_2O_6$ and $CsTiSi_2O_{6.5}$ using the sol-gel method. Both enthalpies of drop solution and unit-cell parameters of the solid solutions show a systematic deviation from linearity. This non-ideal solid solution behavior is probably caused by the varying states of the Si/Al/Ti short-range order across the series. In addition, the enthalpies of formation of these phases, which were derived from their measured enthalpies of drop solution, suggest a destabilizing effect of the substitution $Ti^{4+} + 1/2\ O^{2-} \rightarrow Al^{3+}$ on the pollucite structure.

Acknowledgments This work was supported by the U.S. Department of Energy (DOE) Environmental Management Science Program (EMSP) (Grant No. FG07-97ER45674). Some of the research described in this paper was performed at the Environmental Molecular Sciences Laboratory, a national scientific user facility sponsored by the DOE Office of Biological and Environmental Research and located at PNNL. We thank T.M. Nenoff and M.D. Nyman at the Sandia National Laboratories for their helpful comments.

References

[1]St. V. Naray-Szabo, "Die Struktur des Pollucits $CsAlSi_2O_6 \cdot xH_2O$," *Z. Kristallogr.*, **99**, 277-282 (1938).

[2]W.H. Taylor, "Note on the Structures of Analcite and Pollucite," *Z. Kristallogr.*, **99**, 277-282 (1938).

[3]K. Yanagisawa, M. Nishioka, and N. Yamasaki, "Immobilization of Cesium into Pollucite Structure by Hydrothermal Hot-Pressing," *J. Nucl. Sci. Technol.*, **24** [1], 51-60 (1987).

[4]S.A. Gallagher and G.J. McCarthy, "Preparation and X-ray Characterization of Pollucite ($CsAlSi_2O_6$)," *Inorg. Nucl. Chem.*, **43**, 1773-1777 (1981).

[5]S. Komameni and W.B. White, "Stability of Pollucite in Hydrothermal Fluids," *Sci. Basis Nucl. Waste Manage.*, **3**, 387-396 (1981).

[6]H. Mimura, M. Shibata, and K. Akiba, "Surface Alteration of Pollucite Under Hydrothermal Conditions," *J. Nucl. Sci. Technol.*, **27**, 835-843 (1990).

[7]D. Taylor and C.M.B. Henderson, "The Thermal Expansion of the Leucite Group of Minerals," *Am. Mineral.*, **55**, 1476-1489 (1968).

[8]D.W. Richerson and F.A. Hummel, "Synthesis and Thermal Expansion of Polycrystalline Cesium Minerals," *J. Am. Ceram. Soc.*, **55** [5], 269-273 (1972).

[9]H. Kobayashi, I. Yanase, and T. Mitamura, "A New Model for the Pollucite Thermal Expansion Mechanism," *J. Am. Ceram. Soc.*, **80** [8], 2161-2164 (1997).

[10]P. Cerny, "The Present Status of the Analcime-Pollucite Series," *Can. Mineral.*, **12**, 334-341 (1974).

[11]D.K. Teertstra, B.L. Sherriff, Z. Xu, and P. Cerny, "MAS and DOR NMR Study of Al-Si Order in the Analcime-Pollucite Series," *Can. Mineral.*, **32**, 69-80 (1994).

[12]F. Mazzi, E. Galli, and G. Gottardi, "The crystal structure of tetragonal leucite," *Am. Mineral.*, **61**, 108-115 (1976).

[13]D.R. Peacor, "A high temperature single crystal diffractometer study of leucite, $(K,Na)AlSi_2O_6$," *Zeit. Kristallogr.*, **127**, 213-224 (1968).

[14]R.A. Lange and I.S.E. Carmichael, "Phase Transitions in Leucite ($KAlSi_2O_6$), orthorhombic $KAlSiO_4$, and their iron analogues ($KFeSi_2O_6$, $KFeSiO_4$)," *Am. Mineral.*, **71**, 937-945 (1986).

[15]P.J. Heaney and D.R. Veblen, "A High-Temperature Study of the Low-High Leucite Phase Transition Using the Transmission Electron Microscope," *Am. Mineral*., **75**, 464-476 (1990).

[16]K.D. Hammonds, M.T. Dove, A.P. Giddy, V. Heine, and B. Winkler, "Rigid-Unit Phonon Modes and Structural Phase Transitions in Framework Silicates," *Am. Mineral*., **81**, 1057-1079 (1996).

[17]D.C. Palmer, M.T. Dove, R.M. Ibberson, and B.M. Powell, "Structural Behavior, Crystal Chemistry, and Phase Transitions in Substituted Leucite: High-Resolution Neutron Powder Diffraction Studies," *Am. Mineral*., **82**, 16-29 (1997).

[18]R.E. Newnham, "Crystal Structure and Optical Properties of Pollucite," *Am. Mineral*., **52**, 1515-1518 (1967).

[19]R.F. Martin and M. Lagache, "Cell Edges and Infrared Spectra of Synthetic Leucites and Pollucites in the System $KAlSi_2O_6$ — $RbAlSi_2O_6$ — $CsAlSi_2O_6$," *Can. Mineral*., **13**, 275-281 (1975).

[20]I. Yanase, H. Kobayashi, Y. Shibasaki, and T. Mitamura, "Tetragonal-Cubic Structural Phase Transition in Pollucite by Low-Temperature X-ray Powder Diffraction," *J. Am. Ceram. Soc*., **80** [10], 2693-2695 (1997).

[21]M.L. Balmer, Y. Su, I.E. Grey, A. Santoro, R.S. Roth, Q. Huang, N. Hess, and B.C. Bunker, "The Structure and Properties of Two New Silicotitanate Zeolites," *Mat. Res. Soc. Symp. Proc.*, **465**, 449-455 (1997).

[22]N.J. Hess, M.L. Balmer, and B.C. Bunker, "Ti XAS of a Novel Cs-Ti Silicate," J. *Sol. Sta. Chem.,* **129**, 206-213 (1997).

[23]M.L. Balmer, Q. Huang, W. Wong-Ng. R.S. Roth, and A. Santoro, "Neutron and X-ray Diffraction Study of the Crystal Structure of $CsTiSi_2O_{6.5}$," *J. Sol. Sta. Chem*., **130**, 97-102 (1997).

[24]M.L. Balmer, B.C. Bunker, L.Q. Wang, C.H.F. Peden, and Y. Su, "Solid-State ^{29}Si MAS NMR Study of Titanosilicates," *J. Phys. Chem. B*, **101**, 9170-9179 (1997).

[25]D.E. McCready, M.L. Balmer, and K.D. Keefer, "Experimental and Calculated X-ray Diffraction Data for Cesium Titanium Silicate, $CsTiSi_2O_{6.5}$: A New Zeolite," *Powder Diffraction*, **12** [1], 40-46 (1997).

[26]R.G. Anthony, C.V. Phillip, and R.G. Dosch, "Selective Adsorption and Ion Exchange of Metal Cations and Anions with Silico-Titanates and Layered Titanates," *Waste Management*, **13**, 503-512 (1993).

[27]M.L. Balmer and B.C. Bunker, "*Inorganic ion exchange evaluation and design - silicotitanate ion exchange waste conversion*," Pacific Northwest Laboratory Report No. PNL-10460 (1995).

[28]Y. Su, M.L. Balmer, and B.C. Bunker, "Evaluation of Cesium Silicotitanates as an Alternate Waste Form," *Mat. Res. Soc. Symp. Proc.*, **465**, 457-464 (1996).

[29]Y. Su, M.L. Balmer, L. Wang, B.C. Bunker, M. Nyman, T. Nenoff, and A. Navrotsky, "Evaluation of Thermally Converted Silicotitanate Waste Forms," *Mat. Res. Soc. Symp. Proc.*, **556**, 77-84 (1999).

[30]D.E. Cox, B.H. Toby, and M.M. Eddy, "Acquisition of powder diffraction data with synchrotron radiation," *Aust. J. Phys.*, **41**, 117-131 (1988).

[31]H.M. Rietveld, "A profile refinement method for nuclear and magnetic structure," *J. Appl. Crystallogr.*, **2**, 65-71 (1969).

[32]A.C. Larson and R.B. Von Dreele, "GSAS - General Structure Analysis System," Los Alamos National Laboratory Report No. LAUR 86-748 (1994).

[33]P. Thompson, D.E. Cox, and J. Hastings, "Rietveld refinement of Debye-Scherrer synchrotron X-ray data for Al_2O_3," *J. Appl. Crystallogr.*, **20**, 79-83 (1987).

[34]L.W. Finger, D.E. Cox, and A.P. Jephcoat, "A correction for powder diffraction peak asymmetry due to axial divergence," *J. Appl. Crystallogr.*, **27**, 892-900 (1994).

[35]A. Navrotsky, "Progress and New Directions in High Temperature Calorimetry Revisited," *Phys. Chem. Miner.*, **24**, 222-241 (1997).

[36]M.A. Carpenter, D.C. McConnell, and A. Navrotsky, "Enthalpies of Al/Si Ordering in the Plagioclase Feldspar Solid Solution," *Geochim. et Cosmochim.*, **49**, 947-966 (1985).

[37]R.M. Hazen and A. Navrotsky, "Effects of Pressure on Order-Disorder Reactions," *Am. Mineral.*, **81**, 1021-1035 (1996).

[38]J.R. Goldsmith and F. Laves, "Cation Order in Anorthite ($CaAl_2Si_2O_8$) as Revealed by Gallium and Germanium Substitutions," *Zeit. Kristallogr.*, **106**, 213-226 (1955).

[39]W. Loewenstein, "The Distribution of Aluminum in the Tetrahedra of Silicates and Aluminates," *Am. Mineral.*, **39**, 92-96 (1954).

[40]B.C. Bunker, R.J. Kirkpatrick, and R.K. Brow, "Local Structure of Alkaline-Earth Boroaluminate Crystals and Glasses: I, Crystal Chemical Concepts – Structural Predictions and Comparisons to Known Crystal Structures," *J. Am. Ceram. Soc.*, **74** [6], 1425-1429 (1991).

[41]B.L. Phillips and R.J. Kirkpatrick, "Short-Range Si-Al Order in Leucite and Analcime: Determination of the Configurational Entropy From ^{27}Al and Variable-Temperature ^{29}Si NMR Spectroscopy of Leucite, Its Cs- and Rb-Exchanged Derivatives, and Analcime," *Am. Mineral.*, **79**, 1025-1031 (1994).

[42]B.C. Bunker and M.L. Balmer, "Predicting Structures and Properties of Silicotitanate Materials," unpublished manuscript.

[43]M.A. Hogan and S.H. Risbud, "Gel-Derived Amorphous Cesium-Aluminosilicate Powders Useful for Formation of Pollucite Glass-Ceramics," *J. Mater. Res.*, **6**, 217-219.

[44]H. Xu, A. Navrotsky, M.D. Nyman, and T.M. Nenoff, "Thermochemistry of Microporous Silicotitanate Phases in the Na_2O-Cs_2O-SiO_2-TiO_2-H_2O System," *J. Mater. Res.*, **15**, 815-823.

[45]I. Kiseleva, A. Navrotsky, I.A. Belitsky, and B.A. Fursenko, "Thermochemistry and Phase Equilibria in Calcium Zeolites," *Am. Mineral.*, **81**, 658-667 (1996).

[46]R.L. Putnam, A. Navrotsky, B.F. Woodfield, J. Boerio-Goates, and J.L. Shapiro, "Thermodynamics of Formation for Zirconolite ($CaZrTi_2O_7$) From T = 298.15 K to T = 1500 K," *J. Chem. Thermodynamics*, **31**, 229-243 (1999).

[47]R.A. Robie and B.S. Hemingway, "*Thermodynamic Properties of Minerals and Related Substances at 298.15 K and 1 Bar (10^5 Pascals) Pressure and at Higher Temperatures,*" Geological Survey Bulletin No. 2131 (1995).

[48]K.O. Bennington, R.P. Beyer, and G.K. Johnson, "Thermodynamic Properties of Pollucite (a Cesium-Aluminum-Silicate)," Bureau of Mines Report of Investigations No. 8779 (1983).

Table I. Unit-cell parameters of $CsTi_xAl_{1-x}Si_2O_{6+0.5x}$ pollucites

	synchrotron X-ray		Cu K_α X-ray	
x	*a* (Å)	*V*(Å^3)	*a* (Å)	*V* (Å^3)
0.0	*a*: 13.6731(1)	2559.77(6)		
	c: 13.6921(2)			
0.1			13.703	2573.0
0.2	13.7194(2)	2582.32(9)	13.719	2582.1
0.3			13.729	2587.7
0.4	13.7376(3)	2592.55(16)	13.737	2592.2
0.5			13.746	2597.3
0.6	13.7655(2)	2608.40(12)	13.764	2607.6
0.7			13.777	2615.0
0.8	13.7936(2)	2624.43(10)	13.794	2624.7
0.9			13.815	2636.7
1.0	13.8494(1)	2656.41(7)	13.849	2656.2

Table II. Enthalpies of drop solution in lead borate at 701 °C and enthalpies of formation from the oxides and from the elements at 298 K for $CsTi_xAl_{1-x}Si_2O_{6+0.5x}$ pollucites

x	ΔH_{ds} (kJ/mol)[a]	$\Delta H_{f,ox}^0$ (kJ/mol)	$\Delta H_{f,el}^0$ (kJ/mol)
0.0	244.8 ± 1.5 (7)	-204.3 ± 1.8	-3036.6 ± 2.8
0.1	238.5 ± 2.4 (8)	-197.9 ± 2.6	-3040.8 ± 3.4
0.2	227.8 ± 2.8 (7)	-187.0 ± 3.0	-3040.5 ± 3.7
0.3	225.8 ± 3.3 (10)	-184.9 ± 3.5	-3049.0 ± 4.1
0.4	225.1 ± 2.8 (10)	-184.0 ± 3.0	-3058.7 ± 3.7
0.5	217.7 ± 2.0 (7)	-176.4 ± 2.3	-3061.7 ± 3.1
0.6	213.3 ± 2.6 (8)	-171.9 ± 2.8	-3067.8 ± 3.5
0.7	210.1 ± 1.9 (7)	-168.5 ± 2.2	-3075.1 ± 3.1
0.8	207.5 ± 1.4 (6)	-165.9 ± 1.8	-3083.1 ± 2.8
0.9	199.4 ± 1.9 (7)	-157.6 ± 2.2	-3085.4 ± 3.1
1.0	177.1 ± 2.8 (10)	-135.2 ± 3.0	-3073.6 ± 3.7

[a]Uncertainty is two standard deviations of the mean; value in () is the number of experiments.

Table III. Enthalpies of drop solution in lead borate at 701 °C and enthalpies of formation from elements at 25 °C of several oxides used in calculations of the enthalpies of formation of $CsTi_xAl_{1-x}Si_2O_{6+0.5x}$ pollucites

Oxide	Cs_2O	Al_2O_3	TiO_2	SiO_2
ΔH_{ds} (kJ/mol)	-183.3 ± 1.4[a]	107.9 ± 1.0[b]	55.4 ± 1.2[c]	39.1 ± 0.3[b]
$\Delta H_{f,el}^0$ (kJ/mol)[d]	-346.0 ± 1.2	-1675.7 ± 1.3	-944.0 ± 0.8	-910.7 ± 1.0

[a]From Ref. 44; [b]From Ref. 45; [c]From Ref. 46; [d]From Ref. 47.

Figure Captions

Fig. 1 Crystal structures of the pollucites (A) $CsAlSi_2O_6$ and (B) $CsTiSi_2O_{6.5}$ projected down $[1\,\bar{1}\,1]$. Large spheres represent Cs ions and small ones in (B) represent the positions of the extra oxygens (with an occupancy of 0.060 or 0.023) in excess of 16 oxygens per unit cell; tetrahedra represent $(Si,Al,Ti)O_4$ units. Structural data of (A) are taken from Xu et al. (in prep.) and those of (B) from Ref. 23.

Fig. 2 Variation of cell volume V for the $CsTi_xAl_{1-x}Si_2O_{6+0.5x}$ pollucites as a function of composition. Crosses = synchrotron X-ray data; Diamonds = conventional X-ray data. Errors are smaller than the size of symbols.

Fig. 3 Variation of the enthalpies of drop solution for the $CsTi_xAl_{1-x}Si_2O_{6+0.5x}$ pollucites in lead borate at 701 °C as a function of (A) composition x and (B) cell volume V. The straight line drawn between the data points of the two end-members in (A) represents ideal mixing; the line in (B) is a least squares fit to the data.

Fig. 4 Variation of the enthalpies of mixing for the $CsTi_xAl_{1-x}Si_2O_{6+0.5x}$ pollucites as a function of composition. The line represents ideal mixing.

Fig. 5 Variation of the enthalpies of formation from the oxides for the $CsTi_xAl_{1-x}Si_2O_{6+0.5x}$ pollucites as a function of composition. The line links the data points of the two end-members.

A

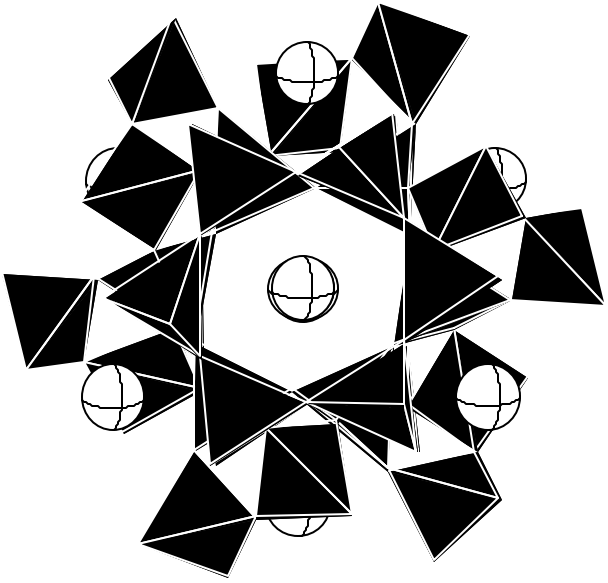

B

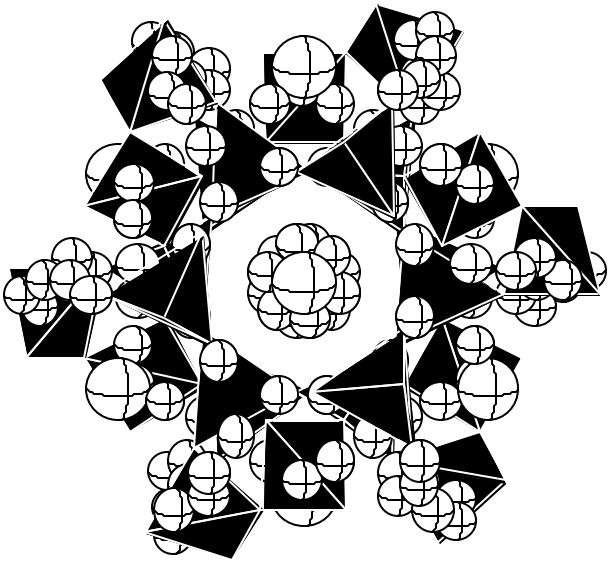

Fig. 1

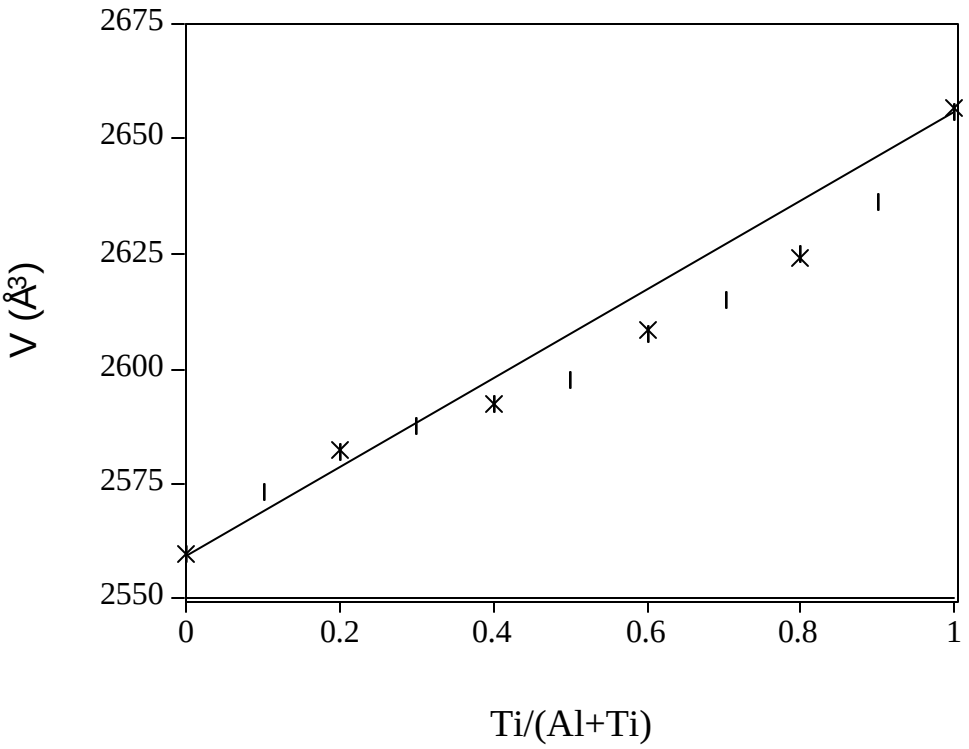

Fig. 2

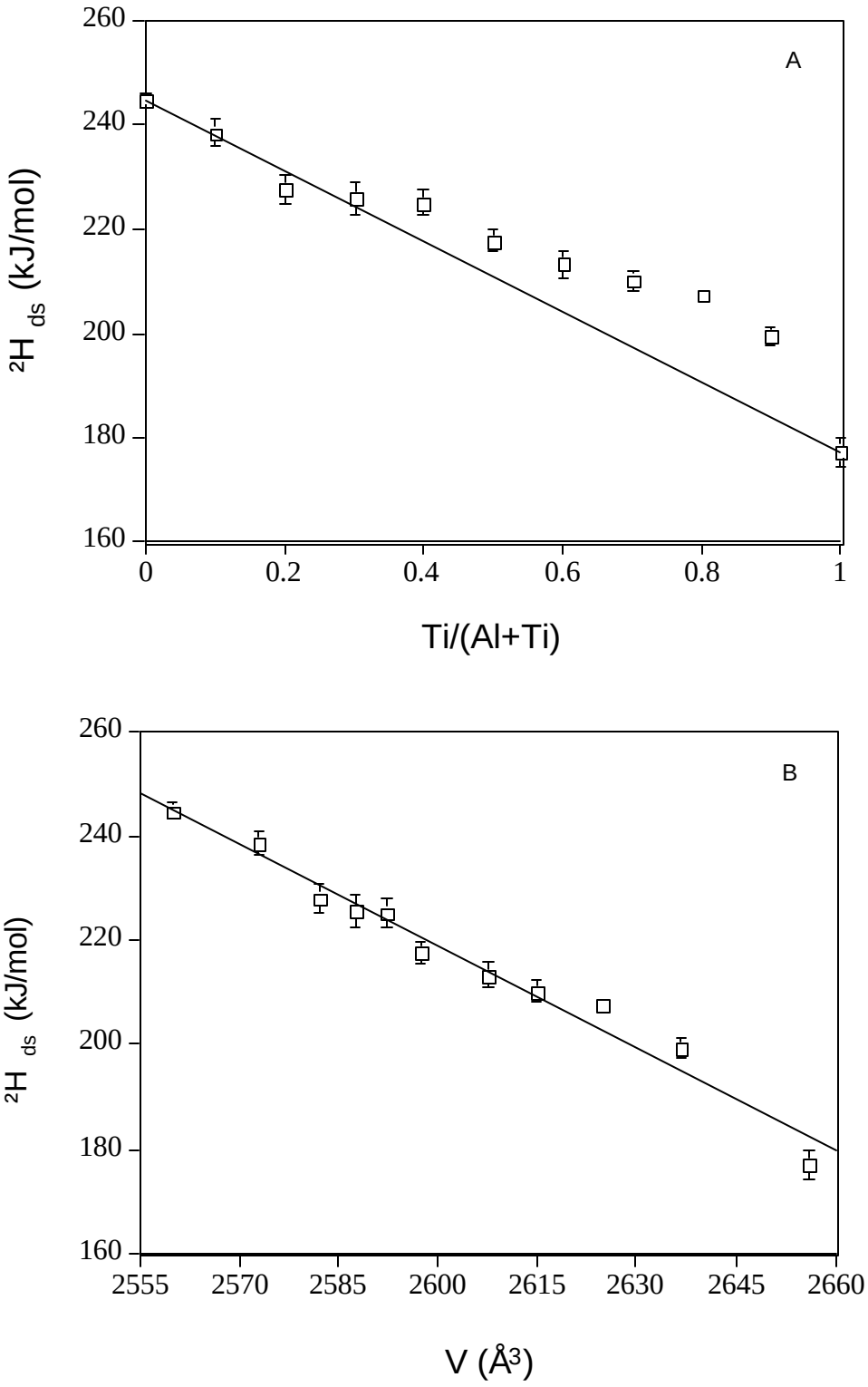
A
260
240
220
200
180
160
0
0.2
0.4
0.6
0.8
1
$^2H_{ds}$ (kJ/mol)
Ti/(Al+Ti)
B
260
240
220
200
180
160
2555
2570
2585
2600
2615
2630
2645
2660
$^2H_{ds}$ (kJ/mol)
V (Å^3)

Fig. 3

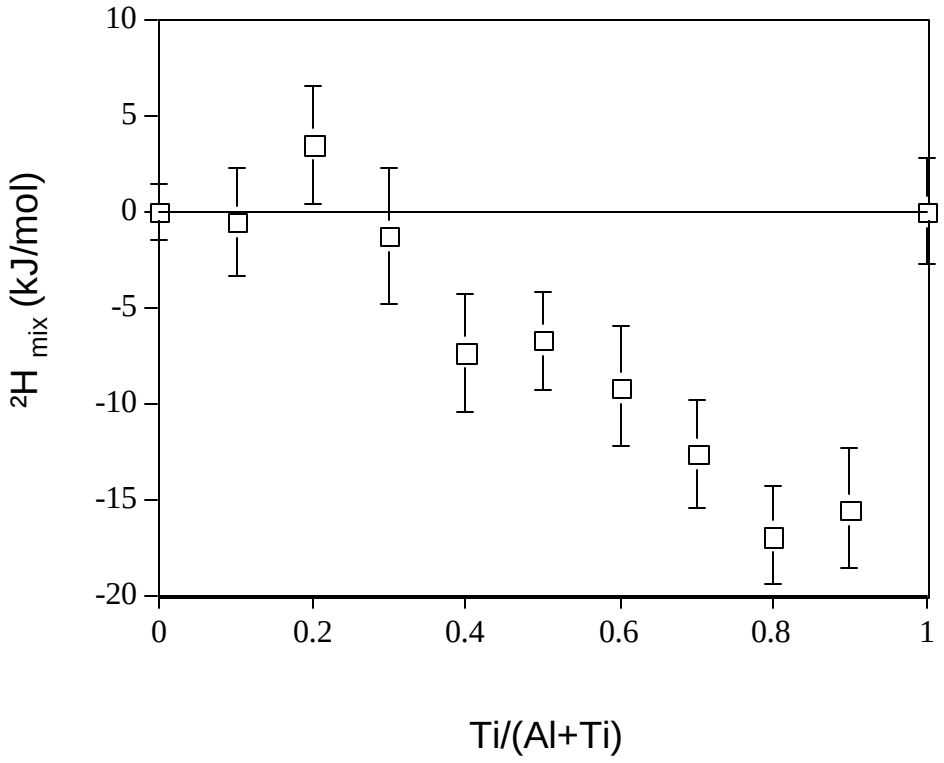

Fig. 4

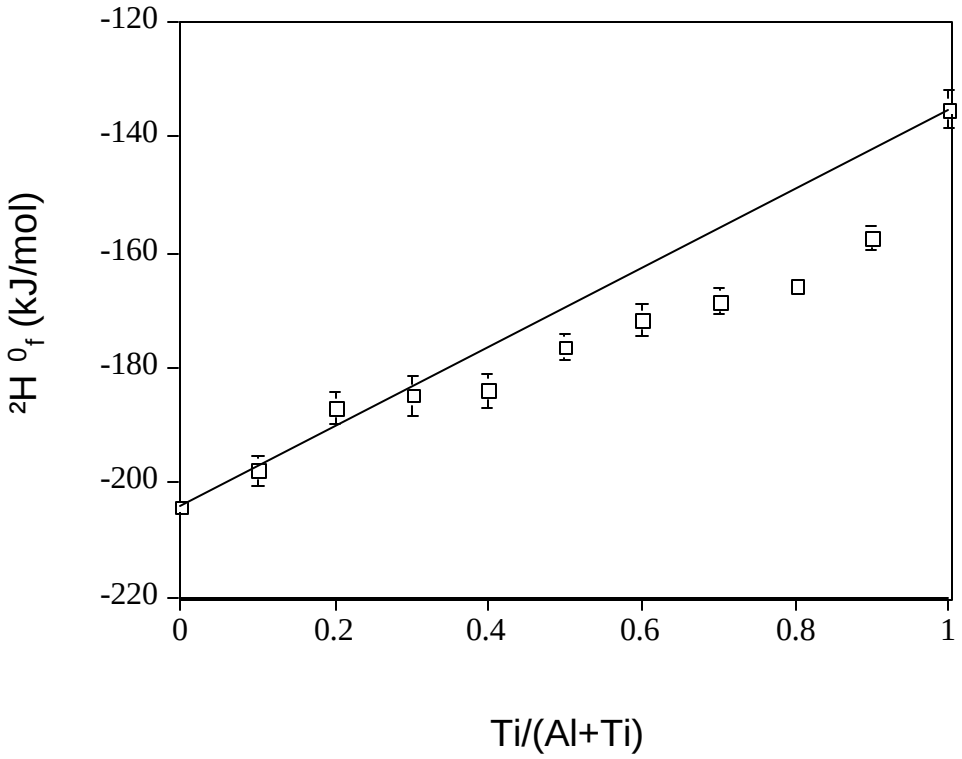

Fig. 5

Integrated Experimental and Computational Methods for Structure Determination and Characterization of a New, Highly Stable Cesium Silicotitanate Phase, $Cs_2TiSi_6O_{15}$ (SNL-A)

M. Nyman[§], F. Bonhomme[§], D. M. Teter[£], R. S. Maxwell[¶], B. X. Gu[†], L. M. Wang[†], R. C. Ewing[†], and T. M. Nenoff [§]*.

[§]Catalysis and Chemical Technologies Department, M.S. 0710

[£]Geochemistry Department, M.S. 0750

Sandia National Laboratories, P.O. Box 5800, Albuquerque, NM 87185

[¶]Lawrence Livermore National Laboratory, Analytical and Nuclear Sciences Division

P.O. Box 808/L-091, Livermore, CA 94551

[†]Department of Nuclear Engineering and Radiological Sciences, University of Michigan, Ann Arbor, MI 48109-2104.

*Author to whom correspondence should be addressed.

Abstract

Exploratory hydrothermal synthesis in the system Cs_2O-SiO_2-TiO_2-H_2O has produced a new polymorph of $Cs_2TiSi_6O_{15}$ (SNL-A) whose structure was determined using a combination of experimental and theoretical techniques (^{29}Si and ^{133}Cs NMR, X-ray Rietveld refinement, and Density Fuctional Theory). SNL-A crystallizes in the monoclinic space-group *Cc* with unit cell parameters: a = 12.998 (2) Å, b = 7.5014 (3) Å, c = 15.156 (3) Å, β = 105.80 (3)°. The SNL-A framework consists of silicon tetrahedra and titanium octahedra which are linked in 3-, 5-, 6-, 7- and 8-membered rings in three dimensions. SNL-A is distinctive from a previously reported *C2/c* polymorph of $Cs_2TiSi_6O_{15}$ by different ring geometries. Similarities and differences between the two structures are discussed. Other characterizations of SNL-A include TGA-DTA, Cs/Si/Ti elemental analyses, and SEM/EDS. Furthermore, the chemical and radiation durability of SNL-A was studied in interest of ceramic waste form applications. These studies show that SNL-A is durable in both radioactive and rigorous chemical environments. Finally, calculated cohesive energies of the two $Cs_2TiSi_6O_{15}$ polymorphs suggest that *Cc* SNL-A phase (synthesized at 200 °C) is energetically more favorable than the *C2/c* polymorph (synthesized at 1050 °C).

Introduction

We are currently studying the viability of silicotitanate phases for cleanup of radionuclides such as ^{90}Sr and ^{137}Cs. Silicotitanate materials of interest include: (1) microporous phases for radionuclide sorption, and (2) condensed, leach resistant phases for radionuclide storage. The ^{137}Cs and ^{90}Sr together compose greater than 99 % of the radioactive inventory of the Hanford wastes, and removal and immobilization of these radionuclides is a primary goal for remediation of this DOE defense waste site.[1,2] A proprietary ion exchanger material jointly developed by Sandia National Laboratories and Texas A & M University, designated crystalline silicotitanate (CST), is currently the best candidate for ^{137}Cs removal.[3-6] Furthermore, its oxide components are suitable for the matrix of a ceramic waste from. Heat treating Cs-loaded CST up to 1000 C results in dehydration and subsequent formation of a mixture of crystalline phases which are very resistant to Cs leaching.[7,8] With the interest of studying the unique durability and stability of silicotitanate phases, a collaborative effort between Sandia National Laboratories (SNL) (hydrothermal synthesis and characterization), Pacific Northwest National Laboratory (PNNL) (solid state synthesis and characterization), and U. C. Davis (calorimetry studies[9] is ongoing to carry out phase searches using component oxides of the Cs-loaded CST material. Current investigations include hydrothermal and solid-state synthesis of ternary Cs_2O-SiO_2-TiO_2-H_2O phases.

Prior to this collaboration, only one ternary Cs_2O-SiO_2-TiO_2-H_2O phase had been reported. This phase is a Cs/Si/Ti pharmacosiderite analogue, $HCs_3Ti_4Si_3O_{16} \cdot 4H_2O$, which is a hydrothermally-synthesized, microporous ion exchanger.[10,11] The efforts of this study have added four additional Cs_2O-SiO_2-TiO_2 phases which include: a) Phases synthesized by solid-state/flux routes at PNNL, $CsTiSi_2O_{6.5}$ (pollucite analogue) and the *C2/c* polymorph of $Cs_2TiSi_6O_{15}$ [12-15] and b) Phases synthesized by hydrothermal routes at SNL, microporous $Cs_3TiSi_3O_{9.5} \cdot 3H_2O$ (SNL-B) [16,17] and the currently reported *Cc* polymorph of $Cs_2TiSi_6O_{15}$ (SNL-A).

The synthesis, structure determination and characterization of the *Cc* polymorph of $Cs_2TiSi_6O_{15}$ is presented in this report. The focus of this body of work is four-fold: 1) hydrothermal synthesis of a new ternary Cs_2O-SiO_2-TiO_2 phase, 2) the integrated use of three techniques (X-ray Rietveld refinement, Density Functional Theory (DFT), and ^{29}Si and ^{133}Cs solid-state NMR) to determine the correct structure of a complex microcrystalline powder phase with 24 independent atoms in the unit cell, 3) comparison of the structure, stability, physical properties and synthesis conditions of *Cc* SNL-A to the *C2/c* polymorph, and 4) examination of the theoretical, chemical and radiation stability of SNL-A, to assess its viability as a waste form phase.

Experimental

General Instrumentation. The **X-ray powder diffraction** pattern of $Cs_2TiSi_6O_{15}$ was measured on a Siemens D500 diffractometer with a Ni-filtered CuKα radiation. The data were collected over the angular range 5-100 ° 2θ with a step size of 0.025 ° and a counting time of 20 seconds per step. The front-loaded sample was rotated at 30

rpm during the measurement. **Magic Angle Spinning Nuclear Magnetic Resonance Spectrometry**: The ^{133}Cs MAS NMR was acquired at 65.6 MHz (11.7T) on a Bruker DRX-500 spectrometer using a Bruker 4 mm CP MAS probe. Sample spinning speed was kept constant at 10 kHz. The ^{133}Cs spectrum was recorded at both fields using a 1-pulse acquire experiment with proton decoupling. Pulse lengths were chosen to be approximately 1/4th of a non-selective $\pi/2$ (~8 μs) pulse, though experiments with variable pulse lengths indicated that all peaks could be characterized by the same nutation behaviour. Solid cesium chloride (223 ppm) and 0.1 M CsCl (0 ppm) were used for external standardization. A 300 second recycle delay was used, and 192 scans were collected. The ^{29}Si MAS NMR was performed at 99.4 MHz on the same Bruker DRX-500 spectrometer and 4 mm probe. The ^{29}Si MAS NMR spectrum was also acquired with 1-pulse acquire experiments though full nonselective $\pi/2$ pulses of 8.5 μs were used. Neat tetramethylsilane (TMS) was used as an external standard (0 ppm) for the ^{29}Si NMR. A recycle delay of 600 seconds was used, and 400 scans were collected. **Inductively Coupled Plasma Spectroscopy (ICP)** for Si and Ti was carried out using an AtomScan-25 ICP-AES instrument, with an argon plasma flame. Samples were dissolved in HF and diluted with water. Reference samples were 10 ppm Si and Ti. Elemental analysis for Cs by **Atomic Adsorption Spectroscopy (AAS)** was performed on a Perkin Elmer 5100 PC AAS instrument. Solutions and standards were prepared with 1000 ppm ionization suppressant. An acetylene/air flame was used for Cs analysis. The **Differential Thermal Analysis-Thermogravimetric Analysis (DTA-TGA)** experiments were performed on a STD 2960 TA DTA-TGA instrument with alumina as a standard for DTA. Samples of SNL-A (10 - 15 mg) were heated at 5 °C/min to 1400 °C with an argon flow of 20 cc/min. **Scanning Electron Microscopy (SEM)** data is collected on a JEOL JSM-T300 SEM with energy dispersive capabilities. **BET surface area** measurements were performed on a Quantachrome Autosorb 6B automated gas sorption system, with adsorbed and desorbed volumes of nitrogen at relative pressures in the range 0.05 to 1.0.

Synthesis of SNL-A. Titanium isopropoxide (TIPT, 0.64 mmol) and tetraethylorthosilicate (TEOS, 5.1 mmol) were combined by stirring and added dropwise to 50% CsOH solution (5.1 mmol) in a 23 ml teflon liner for a Parr pressure reactor. After stirring for approximately 30 minutes, 7.3 mL H_2O was added and the mixture was stirred for 30 minutes more. The final pH of the mixture was approximately 12.7 with a final stoichiometry of $Cs:Ti:Si:H_2O$ = 8:1:8:695. The Parr pressure reactor was placed in a 200 C oven and heated for two weeks. The product was collected by filtration and washed with hot deionized water.

Cesium Leach Tests. The standard PCT (product consistency test) leach test, a common technique developed to evaluate chemical durability of nuclear waste forms in aqueous environments[18,19], was performed on SNL-A. A sample of the material (0.2 g) was placed in a hydrothermal bomb with 10 grams of water at 90 °C for 1, 2, 3, 7, and 10 days. After the designated time of heating, each sample was filtered and the leachate solution was analyzed for Cs concentration by AAS. The solid product was analyzed by XRD to determine if any phase changes had occurred. Surface area of samples for leach rate calculations was determined by BET measurements (29 m^2/g).

Electron Irradiation Studies. Electron irradiation studies of SNL-A were conducted with a JEOL 2000FX transmission electron microscope (TEM) at the University of Michigan. The electron energy used was 200 keV and the sample was irradiated at a dose rate of 5 x 10^{23} electrons / s•cm^2.

Results and Discussion

Synthesis and Bulk Characterizations of SNL-A. Approximately 0.3 g (0.42 mmol) of SNL-A is collected from the synthesis reaction described above. This corresponds with a 66 % yield based on TIPT, the limiting reagent in the synthesis reaction. The reaction is also directly scaleable to obtain more product per synthesis, by utilizing a larger Parr pressure reactor (125 ml teflon liner). Wet chemical analysis for concentrations of Ti (ICP), Si (ICP) and Cs (AA) gave 24.5 wt % Si (calc. 23.3 wt %), 6.77 wt % Ti (calc. 7.25 wt %) and 38.3 wt % Cs (calc. 36.8 wt %). Within experimental error of the analysis techniques (approximately ± 5 %), the product is pure with the stoichiometry $Cs_2TiSi_6O_{15}$. This stoichiometry is also determined by EDS/SEM analysis for Cs, Si and Ti. SNL-A as viewed by SEM is shown in figures 1a and 1b. Figure 1a (1000x magnification) shows the uniformity of the crystallite size and the purity of the sample. Figure 1b (3500x magnification) shows the irregular shape of the crystallites, which are approximately 2 – 5 microns in diameter. No other phases are observed by SEM, which lends further evidence to the formation of a pure material.

Analysis by DTA-TGA reveals a weight loss of less than 1% upon heating to 1400 °C, which indicates SNL-A contains no volatile components such as water molecules or hydroxyl ions. No phase changes are observed by DTA, except an endothermic melting at 1150 °C, which is the same melting temperature observed for the PNNL *C2/c* polymorph of $Cs_2TiSi_6O_{15}$ [20]. Upon melting, SNL-A does not recrystallize. Rather, it solidifies as a glassy material. Furthermore, SNL-A does not undergo any solid-state phase transformations up to its melting point, which suggests it is extremely stable. Additionally, SNL-A heated at 1000 °C for 8 hours did not show any change in its X-ray diffraction pattern.

The PNNL *C2/c* polymorph is synthesized by either high temperature (1050 °C) solid-state reactions of cesium nitrate, titania and silica [20], or grown from the $CsTiSi_2O_{6.5}$ pollucite analogue as a precursor in a cesium vanadate flux at 1100 °C.[14] The SNL-A phase has thus far only been synthesized hydrothermally at 120 – 250 °C. However, since SNL-A cannot be converted to the PNNL phase, the two polymorphs cannot be considered high and low temperature forms. In this study, the energetics of the two phases are compared by DFT total energy calculations (discussed below) Furthermore, calorimetry studies on the two $Cs_2TiSi_6O_{15}$ polymorphs are currently being carried out with Navrotsky et al., and will give more insight into the relative stability of these phases.

Structure Determination and Refinement. Since no single crystal of sufficient size could be grown, the structure of SNL-A had to be solved *ab-initio* from X-ray powder diffraction data. Powder X-ray diffraction data was collected as described above. From that data, the positions of the first 20 Bragg peaks (corrected with Si as external

standard) were used for the indexation with the programs TREOR90[21] and DICVOL91[22]. A satisfactory solution was found in the monoclinic system with approximate cell parameters a = 12.97 Å, b = 7.50 Å, c = 15.15 Å and β=105.70 °, which is similar to those reported for the PNNL phase (a = 13.386(5) Å, b= 7.423(3) Å, c = 15.134(5) Å, β = 107.71(3)° [14]). The extinction laws were consistent with the space-groups *Cc* or *C2/c*. The number of independent Cs and Si sites revealed by the NMR data was only consistent with a structure described in the non centrosymmetric group *Cc.* The correctness of the cell and space group extinctions were checked by a full pattern fitting using the Le Bail method[23], as implemented in the program FULLPROF[24]. No peak was left unaccounted for, thus establishing the validity of the cell and the purity of the sample. The extracted integrated intensities of the peaks below 2θ = 50° were used to solve the structure in the space group *Cc* by direct methods with the program SIR92[25], incorporated in the Wingx[26] suite.

The positions of the cesium atoms and of several of the non-oxygen atoms were directly revealed. The correct assignment of atom types and the completion of the structure were achieved by successive Rietveld refinement using the WinMprof program[27], difference Fourier analysis and "manual" model-building. Although the framework characteristics and topology of the fully refined structure appeared to be essentially correct, the completely free Rietveld refinement of the 70 free atomic positional parameters led to an *unreasonably broad range of Si-O distances*, with a mean value of 1.59 Å and a standard error of 0.13 Å. This imprecision on the oxygen atom positions is partly due to the relative complexity of the structure (24 independent atoms and 70 free positional parameters) and to the strong scattering of the cesium atoms, which tend to overwhelm the contribution of the Si-Ti-O framework. Furthermore, the positions of the non-oxygen atoms can be well described in the centrosymmetric space-group *C2/c* (program MISSYM[28]). About two thirds of the scattering power of the cell are thus related by a pseudo center of symmetry, which tends to introduce high correlation between refined parameters.

In order to obtain a more reasonable structure in the correct (*Cc*) than that achieved by the original free Rietveld refinement as described above, two different approaches were used. The first approach was a Rietveld refinement with soft constraints applied on all 24 independent Si-O distances (Si-O = 1.60 (2) Å). This constrained refinement of the atomic and profile parameters (91 parameters all together) proceeded smoothly down to very satisfactory agreement indices (R_{Bragg}= 3.37%, R_p= 11.73%, χ^2=7.62). No preferred orientation correction was necessary. The Cs sites are fully occupied and no disorder on the Si/Ti sites is evidenced. In comparison with the free refinement, the average shift of the Ti/Si and O atoms from their original positions are 0.05 Å and 0.12 Å respectively, and the Cs atoms are essentially unshifted.

The second approach used was to optimize the atomic coordinates by minimizing the energy of the structure. This work was carried out by Density Function Theory (DFT) using the VASP code developed at the Institut fur Theoretische Physik of the Technische Universitat Wien.[29-32] The quantum mechanical modeling of $CsTi_2Si_6O_{15}$ is a computationally demanding task. The problems of deep pseudopotentials required to accurately model the oxygen

ion, combined with the low symmetry and large unit cell would have made these calculations intractable until recently.

The electronic degrees of freedom were minimized using a residual minimization method direct inversion in the iterative subspace (RMM-DIIS) algorithm.[33,34] The program solves for the electronic charge density using a density functional framework[35,36] within the local density approximation to electron exchange and correlation. The exchange correlation term of the total energy is the Perdew and Zunger parameterization[37] of the Ceperley and Alder data[38]. The electronic wave functions are expanded in a plane wave basis set with periodic boundary conditions. Vanderbilt ultrasoft pseudopotentials were used for the cesium, titanium and oxygen ions with the following states being treated as valence electrons: Cs:$5p^6$ $6s^1$, Ti: $3p^6$ $3d^2$ $4s^2$, and O:$2s^2$ $2p^4$. A norm-conserving pseudopotential was used for silicon with the $3s^2$ $3p^2$ states being treated as valence. The internal coordinates of the initial unit cell derived from the free Rietveld refinement were optimized while keeping the unit cell and cesium ions fixed because of the very low experimental uncertainties on these structural constraints (R_{Bragg}=3.20%). These calculations resulted in optimization of the framework atoms to obtain the most reasonable Si-O/Ti-O bond distances of the three models.

Table 1 shows a comparison of agreement indices for the three models: 1) free Rietveld refinement, 2) Rietveld refinement with Si-O constraint, 3) DFT structural optimization with Cs and unit cell fixed. Although the free Rietveld refinement gave the best agreement indices due to the greatest degrees of freedom on the model, this data set is disregarded for the remainder of the discussion, due to the unreasonable Si-O distances. The crystallographic data and refinement conditions for the "distance constrained" refinement are presented in Table 2; and the observed, calculated and difference plots for this model are shown in figure 2. The structural parameters for two models are

given in Table 3: 1) Rietveld refinement with Si-O constraint, and 2) DFT structural optimization with Cs position and cell parameters fixed. Although atomic positions are very similar for both models, the DFT model gave a more reasonable range of Ti-O distances (1.917 – 1.976 Å) than the Rietveld model with Si-O constraint (1.84 (3) – 2.08 (3) Å). Selected interatomic distances and bond angles from the Rietveld model with Si-O constraint are given in Table 4.

Description of Framework. The composition and melting temperature are identical for SNL-A and the PNNL phase, and the unit cell parameters are quite similar. The calculated powder diffraction patterns of SNL-A and the PNNL phase are shown in figure 3 for comparison. The differences between the diffraction patterns are apparent, confirming there are two distinct polymorphs of $Cs_2TiSi_6O_{15}$. Furthermore, there are distinct differences in the polyhedral rings which make up the silicotitanate framework. SNL-A has six crystallographically unique Si sites, 1 unique Ti site and two unique Cs sites. The PNNL phase is of higher symmetry with 3 unique Si sites, 1 unique Ti site and 1 unique Cs site. For both phases, all TiO_6 octahedra share six corners with SiO_4 tetrahedra, and each SiO_4 tetrahedron is linked to one TiO_6 octahedron and three other SiO_4 tetrahedra. The polyhedra form 3-, 5-, 6-, 7- (SNL-A only) and 8- membered rings that comprise channels in which the cesium cations reside. The ring types which are found in the PNNL and SNL-A phases are summarized in Table 5 for comparison, where Ti is a TiO_6 octahedron, Si(n) is a SiO_4 tetrahedron and $Si(n)_2$ is a Si_2O_7 (n = 1 - 3). The major difference between the two polymorphs is the 7- and 8-membered rings. The PNNL phase has two types of 8-membered rings; one with all SiO_4 tetrahedra and one with 6 SiO_4 tetrahedra and 2 TiO_6 octahedra. SNL-A has only the SiO_4 tetrahedra 8-membered ring, and a unique 7-membered ring (which is not observed in the PNNL phase).

SNL-A viewed down the *a*-axis is shown in figure 4. This projection clearly shows undulating layers of Si_2O_7 [Si(3)-Si(6) and Si(1)-Si(2)] units alternating with layers of titanium octahedra, parallel to the *b*-axis. This view also emphasizes the 5-membered rings composed of four SiO_4 tetrahedra and one TiO_6 octahedron. The 6-membered rings observed in this view are made up of 4 SiO_4 tetrahedra and 2 TiO_6 octahedra. This is a similar view observed in the PNNL phase projected down the *b*-axis.[14]

A view approximately down the (011) axis of SNL-A is shown in figure 5, which is most similar to the (101) view of the PNNL phase.[14] This view reveals the major differences between SNL-A and the PNNL phase. In this projection, an 8-memebered ring, a 7-membered ring and a 3-membered ring are observed. The 3-membered ring consists of one TiO_6 octahedron, an $Si(1)O_4$ and an $Si(3)O_4$ tetrahedron; this 3-membered ring is also present in the PNNL phase. The 8-membered ring consists of eight silicon tetrahedra. The 7-membered ring is not observed in the PNNL phase. Instead, the PNNL phase has a second 8-membered ring consisting of 2 TiO_6 octahedra and 6 SiO_4 tetrahedra. The Cs atoms are located within the 7-membered ring and 8-membered ring channels which run approximately perpendicular to the view shown in figure 5. The shortest Cs-Cs distances are observed within these channels. Cs2 and Cs1 alternate with slightly varying distances of 4.685 (2) Å, 5.105 (2) Å and 4.679 (2) Å. In comparison, the shortest Cs-Cs distances reported for the PNNL phase are 3.765 (2) Å and 4.904 (2) Å.

A second type of 5-ring consisting of 5 SiO_4 tetrahedra is approximately perpendicular to the 8-silicon ring. Both the 5-membered SiO_4 ring and 8-membered SiO_4 ring are emphasized in the view (approximate (101) plane) in figure 6. The 5-membered SiO_4 ring layers alternate with the 8-membered SiO_4 ring layers in a stair-step fashion. A 5-membered SiO_4 ring is also present in the PNNL phase.

^{29}Si and ^{133}Cs MAS NMR. Solid state ^{29}Si and ^{133}Cs MAS NMR analyses of a pure sample of SNL-A gave 6 peaks (~1:1:1:1:1:1 ratio) and 2 peaks (1:1 ratio), respectively. These results played a pivotal role in the final solving and refinement of the structure in the *Cc* space group rather than *C2/c* space group (which has 3 Si and 1 Cs per unit cell). The ^{29}Si and ^{133}Cs NMR plots are shown in figures 7a and 7b, respectively. The ^{29}Si chemical shifts observed for six unique sites range from –96.8 to –110.0 ppm, which is an unusually large shift range for all Q^3 sites (3Si, 1Ti). Furthermore, by conventional Q^x peak assignments, the peak at –110.0 ppm is usually assigned the Q^4 designation.[39] Given these unusual features of the NMR data and the important role the NMR data served in the structure determination, we calculated ^{29}Si shifts using empirical equations first reported by Sherriff [40] and later used specifically for silicotitanates by Labouriau [41]. The ^{29}Si peak shifts were calculated using both data sets: 1) the Rietveld refinement with Si-O constraint and 2) the DFT optimization with Cs and unit cell fixed. These results, along with key structural parameters in the equations, namely the Si(x)-O-Si average bond angle and Si(x)-O-Ti bond angle (x = 1 - 6) are summarized in Table 6. In general, the down field shift increases with increasing average Si(x)-O-X (X=Si, Ti) angle, especially the average Si(x)-O-Si bond angle. The data from the DFT model gave calculated chemical shifts which agree very well with the observed shifts, and the peaks were assigned to crystallographic sites based on this data (see Table 6, column 1). Finally, both sets of calculated ^{29}Si peak shifts show that the large chemical shift range observed for chemically similar (Q^3, 3Si, 1Ti) sites is expected, based on the large range of Si-O-X (X=Si, Ti) bond angles within the framework of SNL-A.

The ^{133}Cs MAS NMR spectrum (figure 7b) shows two unique chemical sites in a 1:1 ratio, which also agrees with the crystallographic data. Figure 8 shows the chemical environments of Cs1 and Cs2, out to the first oxygen coordination spheres. The Cs1 is surrounded by 12 oxygen atoms in the first coordination sphere, and the average Cs-O distance is 3.5 Å. The Cs2 is surrounded by 13 oxygen atoms in the first coordination sphere, and the average Cs-O distance is 3.4 Å. The ^{133}Cs NMR chemical shifts are affected by shielding of the Cs by neighboring atoms; where in general, down field shifts correlate with decreased shielding.[42-44] This suggests the peak at 69.4 ppm corresponds with the Cs2 which has longer Cs-O distances and the peak at 91.8 ppm corresponds the Cs1 with shorter Cs-O bond distances.

Stability of SNL-A. Described below is a summary of experiments executed to determine the energetic stability, and the chemical and radiation stability of SNL-A. These experiments were carried out to investigate the viability of SNL-A as a ceramic waste form phase, such as that which might be formed by thermal conversion of a Cs-exchanged silicotitanate ion exchanger.

Energetics of SNL-A. Using DFT total energy calculations, we optimized the positions of all the ionic coordinates and the shape of the unit cell as a function of volume in order to compare the energetics of the *Cc* and *C2/c* model solutions for SNL-A and that of the PNNL phase. At a given volume, the positions of the cations and the anions were determined by minimizing the Hellmann Feynman forces on the ions. The unit cell edges were determined by making adjustments, until the Pulay corrected stress tensor was zero. The structural parameters were considered to be fully relaxed when the forces on the ions were less that 0.005 eV/A and all stress tensor components were less than 0.001 eV/A^3. Calculations of this type were completed for a variety of volumes for each structure type. The resulting energies were fit to a Birch[45] equation of state

$$E = a_0 + a_1 V^{-2/3} + a_2 V^{-4/3} + a_3 V^{-6/3} \qquad (1)$$

which was used to determine the pressure, the bulk modulus (B_0), and the pressure derivative of the bulk modulus (B'_0). In order to estimate with some degree of confidence the small energy differences between these structures, a kinetic energy cutoff of 500 eV was used. The Brillouin zone integration was completed using a [222] Monkhorst-Pack type grid which reduced to 3 *k*- points in the irreducible Brillouin zone.[46-48] The results of these calculations are shown in the plot in figure 9. These results shows that the *Cc* solution is energetically favorable to the *C2/c* solution for SNL-A. In agreement with the NMR data and Rietveld refinement data, these calculations lended further evidence for the *Cc* model as the correct structure for SNL-A. Finally, the cohesive energy of SNL-A is found to be lower (higher stablility) than the PNNL *C2/c* polymorph.

*Chemical durability of SNL-A***.** SNL-A shows extreme durability in aggressive chemical and radiation environments. The durability of SNL-A with respect to Cs leachability is shown in figure 10, where leach rate is plotted as a function of leach time. Less than 0.2% Cs is lost from the original 37% by weight Cs composition, which translates as essentially no Cs lost due to leaching. Furthermore, SNL-A did not undergo any phase change as a result of the PCT leach tests, as determined by powder X-ray analysis of the leached samples. Furthermore, attempted ion exchange experiments (3 days at 90 °C) in: 1) one molar aqueous sodium chloride solution, and 2) one molar aqueous sodium hydroxide solution, resulted in no ion exchange and no structural change.

Radiation durability of SNL-A . Radiation stability determination of all Cs silicotitanate phases synthesized in the collective (SNL/PNNL/U.C. Davis) studies is important in order to assess the durability of the phases for ion exchange with radionuclides or waste form applications. Electron irradiation with *in situ* TEM studies have proven to be useful in simulating the effects of radiation damage caused by fission products.[16,49,50] SNL-A is extremely radiation resistant. Figure 11 shows the electron diffraction pattern of SNL-A, before and after cumulative radiation

dose of 5 x 10^{23} electrons/cm^2. No changes in the diffraction pattern resulting from irradiation induced amorphization are observed.

Summary and Conclusions

Ternary phase searches by hydrothermal treatment (120 – 200 °C) of Cs_2O-SiO_2-TiO_2-H_2O precursor mixtures has produced a new *Cc* polymorph of $Cs_2TiSi_6O_{15}$ (SNL-A). SNL-A is stable up to its melting temperature at 1150 °C; upon cooling, a glass is formed. No interconversion between the *Cc* –SNL-A and *C2/c* -PNNL polymorphs are observed. The two polymorphs are similar in their unit cell dimensions and identical in melting temperature. However, distinctions are seen in the ring structures. SNL-A possesses a 7-membered ring which is not observed in the *C2/c* -PNNL polymorph, and the *C2/c* -PNNL polymorph has an 8-membered ring which is not found in SNL-A.

The structure of SNL-A is approximately centrosymmetric; the Rietveld refinement of SNL-A powder X-ray diffraction data provided a satisfactory model in the space group *C2/c*. However, both ^{133}Cs and ^{29}Si MAS NMR spectroscopy suggested twice as many unique crystallographic sites for Cs and Si than this solution predicted. DFT total energy calculations were applied to optimize both the *Cc* and *C2/c* model structures. The DFT total energy calculations showed the cohesive energy for the *Cc* solution for SNL-A to be lower than that of the *C2/c* solution, which again suggests the *Cc* solution is correct. This approach gave a solution with better agreement indices, and which agreed with the NMR data. Calculations of theoretical ^{29}Si NMR chemical shifts for SNL-A using both the DFT and Rietveld refinement results showed that the down field chemical shift increases with increasing Si-O-X angle, where X is the neighboring Si or Ti. The chemical shifts calculated from the DFT data agree better with the observed shifts than those calculated from the Rietveld model.

These collective results have shown that use of integrated theory and experiment have allowed us to arrive at a correct structural solution for SNL-A. Specifically, Rietveld structure refinement, Density Functional Theory optimization, and solid state ^{133}Cs and ^{29}Si NMR, were all necessary to obtain the most accurate description of a complex phase (of which single crystals of suitable size cannot be grown) which has a unit cell containing 24 crystallographically unique atoms.

Finally, leach tests and irradiation experiments showed SNL-A to be extremely resistant to both structural damage and Cs loss by either method. These results suggest that SNL-A is a viable silicotitanate phase for ceramic waste forms, such as for sequestration of ^{137}Cs. Furthermore, DFT total energy calculations showed the cohesive energy for *Cc* SNL-A to be lower, and thus energetically favorable within the constraints of the model, relative to the high temperature *C2/c* PNNL polymorph. Since the SNL-A polymorph of $Cs_2TiSi_6O_{15}$ is favored under hydrothermal synthesis conditions (200 °C) and the PNNL polymorph is favored by high temperature routes, it is expected that kinetics rather than thermodynamics dictate the formation of these two phases. For future work, we will investigate

the relative stability of the two $Cs_2TiSi_6O_{15}$ polymorphs using high temperature oxide melt calorimetry[51], where the enthalpies of formation from oxides for these phases can be determined.

Acknowledgements

This work was supported by the U.S. DOE under contracts DE-AC04-94AL85000 (Sandia National Laboratories) and W-7405-Eng-48 (University of California Lawrence Livermore National Laboratory).

.

All authors thank the DOE Environmental Management Science Program (EMSP) for funding for this work under separate grants for the University of Michigan and SNL (EMSP grant DE-FG07-97ER45652 at the University of Michigan; project # 27601 at SNL).

We thank Dr. Todd Alam at Sandia National Laboratories for the preliminary NMR spectroscopy experiments, and M. Lou Balmer (PNNL), Yali Su (PNNL), Alex Navrotsky (U.C. Davis) and Hongwu Xu (U. C. Davis) for helpful discussions.

Table 1. Comparison of agreement indices for the three models.

Model	R_{Bragg}	R_p	R_{wp}	c^2
Free Rietveld refinement	3.20	11.63	15.56	7.53
Rietveld refinement with Si-O constraint	3.37	11.73	15.69	7.62
DFT model with Cs positions and unit cell fixed by free Rietveld refinement	4.53	12.53	16.37	8.05

Table 2. Crystallographic Data for SNL-A

Chemical Formula		$Cs_2TiSi_6O_{15}$
M(g/mol)		722.2
Crystal System		Monoclinic
Space Group	**Cc *(#9)***	
a (Å)		12.988 (2)
b (Å)		7.5014 (3)
c (Å)		15.156 (3)
β		105.80 (3)
Volume ($Å^3$)		1420.8 (7)
Z		4
D_c (g/cm^3)		3.376
λ		Cu $K_{\alpha1}$, $K_{\alpha2}$
Geometry		Bragg-Brentano
Range 2θ (°)		5.00 – 100.00
Step size (°)		0.025
Time per step (s)		20
No. free parameters		91
No. of structural parameters		74
No. “independent” reflections		736
Number of soft constraints		24
Minimum FWHM (°)		0.11
R_I (%)		3.37
R_{wp} (%)		15.69
χ^2		7.62

Table 3 Structural parameters for two models.

	Rietveld refinement with Si-O constraints (1.60 (2) Å)			DFT model using unit cell and Cs coordinates from the free Rietveld refinement		
atom	**x (esd)**	**y (esd)**	**z (esd)**	**x**	**y**	**z**
Cs1	0.25970 (fixed)	0.3658 (8)	0.48146 (fixed)	0.25970	0.36710	0.48146
Cs2	0.2832 (3)	0.1337 (8)	0.8030 (3)	0.28440	0.13450	0.80406
Ti	0.539 (1)	0.240 (1)	0.400 (1)	0.53740	0.24215	0.40110
Si1	0.006 (1)	0.068 (2)	0.249 (1)	0.00110	0.07082	0.25206
Si2	0.057 (1)	0.032 (2)	0.563 (1)	0.05177	0.02796	0.56566
Si3	0.084 (1)	0.444 (2)	0.242 (1)	0.08308	0.45208	0.24143
Si4	0.257 (1)	0.113 (2)	0.056 (1)	0.25245	0.12034	0.05332
Si5	0.322 (1)	0.328 (2)	0.241 (1)	0.31768	0.34226	0.24053
Si6	0.484 (1)	0.074 (2)	0.039 (1)	0.47898	0.07257	0.03624
O1	0.000 (2)	0.124 (4)	-0.002 (1)	0.00000	0.13127	0.00000
O2	0.015 (2)	0.282 (3)	0.261 (2)	0.01025	0.28633	0.25821
O3	0.051 (2)	0.499 (5)	0.136 (2)	0.04866	0.50803	0.13532
O4	0.051 (2)	0.004 (5)	0.166 (2)	0.04979	0.00408	0.17055
O5	0.183 (2)	0.043 (4)	0.576 (2)	0.17949	0.04511	0.57225
O6	0.207 (2)	0.376 (4)	0.262 (2)	0.20523	0.38197	0.26171
O7	0.298 (2)	0.230 (5)	0.146 (2)	0.29846	0.22400	0.14911
O8	0.360 (2)	0.032 (3)	0.027 (2)	0.35342	0.03045	0.02647
O9	0.381 (2)	0.516 (4)	0.236 (2)	0.37190	0.52947	0.22141
O10	0.399 (2)	0.246 (4)	0.332 (2)	0.39077	0.24424	0.32800
O11	0.492 (2)	0.288 (3)	0.030 (2)	0.49162	0.28687	0.03043
O12	0.521 (2)	0.022 (3)	0.461 (2)	0.51437	0.01981	0.45538
O13	0.564 (2)	0.472 (3)	0.341 (1)	0.55830	0.47240	0.34501
O14	0.581 (2)	0.112 (3)	0.304 (2)	0.58085	0.11315	0.30808
O15	0.698 (2)	0.255 (3)	0.478 (2)	0.68731	0.25573	0.47277

Table 4. Selected bond angles and distances for SNL-A from the Rietveld refinement with Si-O constraints (1.60 (2) Å).

Atom A	$O(x)_1$	A-$O(x)_1$ bond length (Å) (esd)	$O(x)_2$	$O(x)_1$-A-$O(x)_2$ bond angle (°) (esd)	Atom A	$O(x)_1$	A-$O(x)_1$ bond length (Å) (esd)	$O(x)_2$	$O(x)_1$-A-$O(x)_2$ bond angle (°) (esd)
Ti	O1	1.97 (3)	O10	89.6 (1.5)	**Si3**	O2	1.59 (2)	O3	111.5 (2.1)
	O10	1.84 (3)	O12	93.4 (1.3)		O3	1.59 (2)	O6	104.8 (1.8)
	O12	1.92 (3)	O14	92.4 (1.2)		O6	1.62 (2)	O14	109.0 (1.8)
	O13	2.02 (3)	O14	89.0 (1.3)		O14	1.58 (2)	O2	113.1 (1.8)
	O14	1.95 (3)	O15	90.7 (1.4)		O2		O6	107.7 (1.9)
	O15	2.08 (3)	O1	88.3 (1.3)		O3		O14	110.4 (2.0)
	O1		O12	89.2 (1.4)	**Si4**	O7	1.59 (2)	O8	109.3 (1.8)
	O1		O13	89.4 (1.2)		O8	1.62 (2)	O5	111.0 (1.8)
	O10		O13	88.8 (1.3)		O5	1.60 (2)	O15	114.2 (1.8)
	O10		O14	91.3 (1.4)		O15	1.58 (2)	O7	106.3 (2.1)
	O12		O15	90.7 (1.2)		O7		O5	108.2 (2.3)
	O13		O15	87.1 (1.2)		O8		O15	107.8 (1.9)
Si1	O2	1.61 (2)	O4	111.3 (2.2)	**Si5**	O6	1.64 (2)	O7	108.3 (1.9)
	O4	1.60 (2)	O9	113.7 (2.0)		O7	1.57 (2)	O9	109.7 (2.1)
	O9	1.62 (2)	O13	102.6 (1.7)		O9	1.62 (2)	O1	100.5 (1.8)
	O13	1.58 (2)	O2	110.1 (1.8)		O10	1.58 (2)	O6	108.4 (2.0)
	O2		O9	106.7 (1.6)		O6		O9	106.8 (1.7)
	O13		O4	111.9 (1.8)		O7		O10	122.0 (2.1)
Si2	O5	1.60 (2)	O11	115.6 (1.8)	**Si6**	O8	1.62 (2)	O11	105.3 (1.6)
	O11	1.60 (2)	O1	108.2 (1.8)		O11	1.62 (2)	O3	113.8 (2.2)
	O1	1.58 (2)	O4	110.5 (2.2)		O3	1.59 (2)	O12	109.7 (1.9)
	O4	1.60 (2)	O5	102.1 (1.8)		O12	1.56 (2)	O8	108.8 (1.7)
	O5		O1	113.5 (1.8)		O8		O3	108.2 (1.8)
	O11		O4	106.7 (2.2)		O11		O12	110.8 (2.0)

Cs-O Distances (Å)

Cs1	O(x)	distance	O(x)	distance	**Cs2**	O(x)	distance	O(x)	distance
	O1	3.07 (3)	O9	3.85 (3)		O2	3.30 (3)	O9	3.20 (3)
	O2	3.99 (3)	O10	3.88 (4)		O4	3.33 (3)	O10	3.20 (3)
	O5	3.11 (3)	O11	3.89 (3)		O5	3.40 (3)	O11	3.93 (3)
	O6	3.21 (3)	O12	3.26 (3)		O6	3.82 (3)	O12	3.55 (3)
	O7	3.88 (4)	O14	3.56 (3)		O7	3.66 (4)	O13	3.16 (3)
	O8	3.25 (3)	O15	3.02 (2)		O8	3.36 (3)	O14	3.24 (3)
								O15	3.24 (2)

Table 5.

Comparison of Rings of the PNNL and SNL-A Polymorphs of $Cs_2TiSi_6O_{15}$

Phase [building blocks]	**Ring type**	**Ring polyhedra**
	3-ring	Si(2)-Si(4)-Ti
SNL-A $Cs_2TiSi_6O_{15}$		Si(1)-Si(6)-Ti
(*Cc* polymorph)	5-ring	Si(2) -Si(1) -Si(5) -Si(4) -Si(6)
[$Si(1)O_4$, $Si(2)O_4$, $Si(3)O_4$,		Si(2) -Si(1) -Si(3) -Si(5) -Si(6)
$Si(4)O_4$, $Si(5)O_4$, $Si(6)O_4$, TiO_6]	5-ring	Ti-Si(6)-Si(3) -Si(1) -Si(2)
		Ti-Si(1) -Si(2) -Si(6) -Si(3)
	6-ring	Ti-Si(2) -Si(6) -Ti-Si(3) -Si(1)
	7-ring	Ti-Si(3) -Si (5) -Ti-Si (2) -Si(6) -Si(4)
		Ti-Si(6) -Si (4) -Ti-Si (1) -Si(3) -Si(5)
	8-ring	Si(6)-Si(2)–Si(4)-Si(6)-Si(3)-Si(1)-Si(5)-Si(3)
	3-ring	Si(2)-Si(3)-Ti
PNNL $Cs_2TiSi_6O_{15}$[14]	5-ring	Si(2)-Si(3)-Si(1)-Si (2)-Si(3)
(*C2/c* polymorph)	5-ring	Ti Si(2) Si(3) $Si(1)_2$
[$Si(1)_2O_7$, $Si(2)O_4$,	6-ring	Ti Si(1) Si(3) Ti Si(1) Si(3)
$Si(3)O_4$, TiO_6]	8-ring	$Si(1)_2$-Si(2) -Si(3) -$Si(1)_2$-Si(3) -Si(2)
	8-ring	Ti-Si(2) -Si(1) -Si (3) -Ti-Si(2) -Si(1) -Si(3)

Table 6. Observed and calculated ^{29}Si NMR shifts and related structural data for SNL-A.

Observed ^{29}Si NMR peak shifts			^{29}Si NMR peak shifts calculated from DFT model data			^{29}Si NMR peak shifts calculated from Rietveld refinement data		
Si (x)	δ_{obs} (ppm)	Peak integation (% of total)	δ_{calc} (ppm)	Avg. Si(x)-O-Si(y) angle (°)	Si(x)- O-Ti angle (°)	δ_{calc} (ppm)	Avg. Si(x)-O-Si(y) angle (°)	Si(x)- O-Ti angle (°)
Si(1)	-96.8	16.3	-95.1	140	135	-94.9	145	133
Si(4)	-97.8	19.6	-96.0	141	134	-96.2	145	132
Si(2)	-100.2	17.9	-97.7	142	134	-97.5	144	134
Si(5)	-102.4	15.5	-101.6	147	139	-106.9	154	154
Si(6)	-107.3	15.5	-106.5	150	146	-107.1	154	143
Si(3)	-110.0	15.2	-109.6	154	156	-107.8	150	149

Figure Captions

Figure 1. Scanning electron micrographs of SNL-A at 1000x magnification (left) showing the uniformity and purity of the sample; and 3500x magnification (right) illustrating the irregular crystallite shape.

Figure 2. Calculated, observed, and difference profiles for the Rietveld refinement of SNL-A in the *Cc* space group.

Figure 3. Calculated diffraction patterns for the PNNL (top) and SNL-A (bottom) polymorphs of $Cs_2TiSi_6O_{15}$.

Figure 4. View of SNL-A, approximately down the *a*-axis, emphasizing the 5-rings (1Ti, 4Si) and 6-rings (2Ti, 4Si).

Figure 5. View of SNL-A, approximately along (011). This view reveals a 3-ring (1Ti, 3Si), an 8-ring (8Si) and a 7-ring (2Ti, 5Si). The shortest Cs-Cs distances are found in the channels formed by the 7-rings and 8-rings.

Figure 6. View of SNL-A showing the approximately perpendicular layers of 8-rings (8Si) and 5-rings (5Si).

Figure 7. a) ^{133}Cs MAS NMR of SNL-A showing two unique Cs sites in a 1:1 ratio.
* indicates spinning side bands. b) ^{29}Si MAS NMR of SNL-A showing 6 unique Si Q^3 (3Si, 1Ti) sites in ~1:1:1:1:1:1 ratio.

Figure 8. View of Cs1 and Cs2 showing coordination environments.

Figure 9. Cohesive energy (eV/primitive cell) as a function of primitive unit cell volume, calculated for the SNL-A *Cc* solution, the SNL-A *C2/c* solution, and the *C2/c* PNNL $Cs_2TiSi_6O_{15}$.

Figure 10. Product consistency test (PCT) leach test for SNL-A showing Cs leach rate as a function of time.

Figure 11. Electron diffraction pattern of SNL-A before and after cumulative radiation dose of 5 x 102^3 electrons/cm^2. No changes in the electron diffraction pattern resulting from irradiation induced amorphization are observed.

References

1) Wilson, E. K. *Chem. Eng. News* **1997**, 30.
2) Illman, D. L. *Chem. Eng. News* **1993**, 9.
3) Nenoff, T. M.; Thoma, S. G.; Krumhansl, J. L., SAND96-2580: "The Stability and Selectivity of TAM5: A Silicotitanate Molecular Sieve for Radwaste Clean-up," Sandia National Laboratories, 1996.
4) Poojary, D. M.; Cahill, R. A.; Clearfield, A. *Chem. Mater.* **1994**, *6*, 2364.
5) Anthony, R. G.; Phillip, C. V.; Dosch, R. G. *Waste Management* **1993**, *13*, 503.
6) Anthony, R. G.; Dosch, R. G.; Gu, D.; Philip, C. V. *Ind. Eng. Chem. Res.* **1994**, *33*, 2702.
7) Su, Y.; Balmer, M. L.; Wang, L.; Bunker, B. C.; Nenoff, T. M.; Nyman, M.; Navrotsky, A., *"Evaluation of Thermally Converted Silicotitanate Waste Forms"* : Boston, MA, 1998, p 77.
8) Su, Y.; Balmer, M. L.; Bunker, B. C., *"Evaluation of Cesium Silicotitanates as an Alternative Waste Form"* : Boston, MA, 1997, p 457.
9) Xu, H.; Navrotsky, A.; Nyman, M.; Nenoff, T. M. *J. Mater. Res.* **2000**, *15*, 815.
10) Behrens, E. A.; Poojary, D. M.; Clearfield, A. *Chem. Mater.* **1996**, *8*, 1236.
11) Behrens, E. A.; Clearfield, A. *Micropor. Mater.* **1997**, *11*, 65.
12) Balmer, M. L.; Su, Y.; Grey, I. E.; Santoro, A.; Roth, R. S.; Huang, Q.; Hess, N.; Bunker, B. C., *"The Structure and Properties of Two New Silicotitanate Zeolites"* : Boston, MA, 1997, p 449.
13) Balmer, M. L.; Huang, Q.; Wong-Ng, W.; Roth, R. S.; Santoro, A. *J. Sol. State Chem.* **1997**, *130*, 97 .
14) Grey, I. E.; Roth, R. S.; Balmer, M. L. *J. Sol. State Chem.* **1997**, *131*, 38.
15) McCready, D. E.; Balmer, M. L.; Keefer, K. D. *Powder Diffract.* **1997**, *12*, 40.
16) Nyman, M.; Nenoff, T. M.; Gu, B.; Wang, L.; Ewing, R. C. *J. Microporous and Mesoporous Mater.* **submitted 2000**.

17) Nyman, M.; Nenoff, T. M.; Su, Y.; Balmer, M. L.; Navrotsky, A.; Xu, H., *"New Crystalline Silicotitanate (CST) Waste Forms: Hydrothermal Synthesis and Characterization of Cs-Si-Ti-O Phases"* : Boston, MA, 1998, p 71.

18) Li, H.; Tomozawa, M. *J. Non-cryst. Sol.* **1996**, *195*, 188.

19) Mesko, M. G.; Day, D. E. *J. Nucl. Mater.* **1999**, *273*, 27.

20) Su, Y., personal communication.

21) Werner, P. E.; Eriksson, J.; Westdahl, J. *J. Appl. Cryst.* **1985**, *18*, 367.

22) Boultif, A.; Louer, D. *J. Appl. Cryst.* **1991**, *24*, 987.

23) LeBail, A.; Duroy, H.; Fourquet, J. *Mater. Res. Bull.* **1988**, *23*, 447.

24) Rodriguez-Carvajal, J., *"Collected Abstracts of Powder Diffraction Meeting"* : Toulouse, France, 1990, p 127.

25) Altomare, A.; Cascarano, G.; Giacovazzo, C.; Guagliardi, A.; Burla, M. C.; Polidori, G.; Carnalli, M. *J. Appl. Cryst.* **1994**, *27*, 435.

26) Farrugia, L. J. *J. Appl. Cryst.* **1999**, *32*, 837.

27) Jouanneaux, A. *CPD Newsletter* **1999**, *21*, 13.

28) LePage, Y. *J. Appl. Cryst.* **1987**, *20*, 264.

29) Kresse, G.; Furthmuller, J. *Comp. Mat. Sci.* **1996**, *6*, 15.

30) Kresse, G.; Hafner, J. *Phys. Rev. B* **1993**, *47*, 558.

31) Kresse, G.; Hafner, J. *Phys. Rev. B* **1994**, *49*, 14251.

32) Kresse, G.; Furthmuller, J. *Phys. Rev. B* **1996**, *54*, 11169.

33) Pulay, P. *Chem. Phys. Lett.* **1980**, *73*, 393.

34) Wood, D. M.; Zunger, A. *J. Phys. A* **1985**, *18*, 1343.

35) Hohenberg, P.; Kohn, W. *Phys. Rev.* **1964**, *136*, 864.

36) Kohn, W.; Sham, L. J. *Phys. Rev.* **1965**, *140*, 1133.

37) Perdew, J. P.; Zunger, A. *Phys. Rev. B* **1981**, *23*, 5048.

38) Ceperley, D. M.; Alder, B. J. *Phys. Rev. Lett.* **1980**, *45*, 566.

39) Balmer, M. L.; Bunker, B. C.; Wang, L. Q.; Peden, C. H. F.; Su, Y. *J. Phys. Chem. B* **1997**, *101*, 9170.

40) Sherriff, B. L.; Grundy, H. D. *Nature* **1988**, 819.

41) Labouriau, A.; Higley, T. J.; Earl, W. L. *J. Phys. Chem.* **1998**, *102*, 2897.

42) Malek, A.; Ozin, G. A.; Macdonald, P. M. *J. Phys. Chem.* **1996**, *100*, 16662.

43) Ahn, M. K.; Iton, L. E. *J. Phys. Chem.* **1991**, *95*, 4496.

44) Yagi, F.; Kanuka, N.; Tsuji, H.; Nakata, S.; Kita, H.; Hattori, H. *Micropor. Mater.* **1997**, *9*, 229.

45) Birch, F. *J. Geophys. Res.* **1978**, *83*, 1257.

46) Bouckaert, L. P.; Smoluchowski, R.; Wigner, E. *Phys. Rev.* **1936**, *50*, 58.

47) Monkhorst, H. J.; Pack, J. D. *Phys. Rev. B.* **1976**, *13*, 5188.

48) Evarestov, R. A.; Smirnov, V. P. *Phys. Stat. Sol.* **1983**, *119*, 9.

49) Wang, L. M.; Wang, S. X.; Ewing, R. C., *"Radiation Effects in Zeolite: Relevance to near-field contamination"* : Las Vegas, NV, 1997, p 772.

50) Wang, L. M.; Wang, S. X.; Gong, W. L.; Ewing, R. C.; Weber, W. J. *Mater. Sci. Eng.* **1998**, *A253*, 106.

51) Navrotsky, A. *Phys. Chem. Miner.* **1997**, *24*, 222.

From Octahedral Molecular Sieves to Perovskites: Rational Design of New Materials for Sequestration and Immobilization of Hazardous Metals

May Nyman*, Akhilesh Tripathi[†], John B. Parise[†,‡], Robert S. Maxwell[§], William T. A. Harrison[||] and Tina M. Nenoff[¶]*

*Catalysis and Chemical Technologies Department, M.S. 0710
Sandia National Laboratories, P.O. Box 5800, Albuquerque, N.M. 87185-0710

[†]Department of Chemistry and [‡]Department of Geosciences,
State University of New York, Stony Brook, NY 11794-2100

[§]Lawrence Livermore National Laboratory, P.O. Box 808, L-226,
Livermore, California 94551

[||]Department of Chemistry, University of Aberdeen
Aberdeen AB24 3UE, United Kingdom

[¶]Author to whom correspondence should be addressed

Ion exchangers for scavenging hazardous metals from industrial[1-4] and nuclear waste[5-8] streams become increasingly desirable as worldwide technological development escalates. While synthesizing new materials for ion exchange is common, tailoring optimum ion exchange properties by rational design is exceptional.[9-11] We have strategically developed a new class of niobate-based materials which function to both sequester and immobilize[12-16] hazardous divalent metals (i.e. Cd^{2+}, Ni^{2+}, Zn^{2+}, $^{90}Sr^{2+}$) by selective ion exchange and subsequent thermal alteration to stable

perovskite-type phases. We designed these materials by extrapolating to alternative chemical systems the rationale that explains framework topology of zeolites.[17] Substitution of Al^{III} into an $Si^{IV}O_2^{4-}$ tetrahedron in a zeolite framework imparts a net negative charge, requiring a charge-balancing cation which simultaneously promotes open-framework growth. Likewise, substitution of Ti^{IV}/Zr^{IV} for Nb^{V} in the $NaNbO_3$ structure, charge-balanced by a sodium, produced SOMS (Sandia Octahedral Molecular Sieves)[18]. SOMS are structurally unique with sodium occupying both channel and framework[19] sites, a feature observed prior only in lithosilicates[20-21]. The SOMS formed by this potentially universal approach compose an unprecedented class of the octahedral molecular sieves, previously represented by manganates only[22-24].

The SOMS phases are synthesized by hydrothermal treatment of extremely basic sol mixtures containing water, sodium hydroxide, and hydrolyzed metal (Nb, Ti, Zr) alkoxides. The M^{IV}:Nb ratio (M = Ti, Zr) in the resultant SOMS phase is directly correlated with the precursor ratio for the range of 1:50 – 1:4 M:Nb. Within this composition range, isostructural materials are formed, based on powder X-ray diffraction analysis. Thus, members of the SOMS family are described as x%-Na/M^{IV}/Nb -SOMS where $x = 100x[M^{IV}] / [M^{IV} + Nb]$. The 20%-Na/$Ti^{IV}$/Nb -SOMS (SOMS-1) is the composition most readily obtained in its pure form. Precursor sols with lower concentrations of titanium or zirconium (x < 20%) tend to crystallize as perovskite or illmenite upon hydrothermal treatment. However, addition of 2,4-pentadionate to the reaction mixtures provides pure samples of SOMS with x<20% consistently, and hence systematic compositional variation is readily achievable. Higher concentrations of the titanium (>1:4 Ti:Nb ratio) in the precursor sol results in formation of the SOMS-1 phase, along with some titanium-rich, amorphous impurities. This suggests 20 % is the maximum possible substitution of M^{IV} into the framework niobium site. However, syntheses with increasing Ti:Nb (up to 2:1) ratio produces larger crystals with a less needle-like morphology (figure 1), which provided weakly diffracting crystals (5x8x8 μm) suitable only for single-crystal data collection at an X-ray synchrotron source.

A combination of analytical and spectroscopic data (DTA-TGA, ICP-AES, ^1H solid-state MAS NMR) led us to a fixed composition for SOMS-1 of $Na_{16}Ti_{3.2}Nb_{12.8}O_{44.8}(OH)_{3.2}\cdot 8H_2O$, which gave a satisfactory crystallographic solution with a discrepancy index of R_1 = 6.29 % for the single crystal structure determination. To ensure the single crystal structure determination was representative of the bulk SOMS-1 sample, synchrotron X-ray powder

diffraction data were collected and modeled by the Rietveld method. The excellent agreement indicates that indeed the models derived from single crystal and powder data are equivalent. The structure of SOMS-1 is viewed down the *b*-axis in figure 2. In this chemically-constrained model, 3.2Ti and 12.8Nb atoms per unit cell distribute statistically over two crystallographically independent Ti/Nb-sites. The octahedrally coordinated Na1 and Na2 sites and the square planar Na3 site are fully occupied, consistent with 5:1:4 Na:Ti:Nb ratio observed by chemical analysis (ICP-AES). The geometry of the Na3 site is distorted by displacements away from the square planar position in the direction of the *b*-axis, giving rise to 50% occupied sites 0.52 Å above and below the plane of the oxygen atoms. Although such coordination is unusual for Na^+, it is not unprecedented and is likely a compromise to the restricted coordination geometry provided by the framework.[25] The ^{23}Na MAS NMR analysis confirmed two Na geometries in a 3:1 ratio (octahedral:distorted square planar) at -8 ± 1 ppm (octahedral) and -11 ± 2 ppm (distorted square planar).

The overall architecture of SOMS-1 is a 3-dimensional framework with 1-dimensional channels oriented parallel to the *b*-axis, and three distinct structural units. The first unit is edge-sharing double chains of Nb/Ti octahedra containing out-of-center atoms common to Ti/Nb chemistry[26] which run parallel to [010]. The second building unit is a layer of Na-centered polyhedra consisting of edge-linked, six coordinated Na1 and Na2 atoms. The framework then consists of sheets of these Na-layers alternating with layers containing the double chains of Ti/Nb octahedra. The third structural unit, the Na3 site, resides between these double chains.

The SOMS phases exhibit extreme exchange selectivity for divalent cations over monovalent cations. The distribution coefficients (K_d) for a variety of hazardous industrial metals, the alkali metals and the alkaline earth metals on the 12%-Na/Zr^{IV}/Nb-SOMS and SOMS-1 phases are summarized in Table I, where K_d[27] is the ratio of metal adsorbed onto the ion exchanger to the metal remaining in solution. Most of the divalent transition metals as well as the Ba^{2+} and Sr^{2+} are completely removed from solution by both SOMS phases. Selectivity of the SOMS phases (directly correlated with K_d) for the monovalent alkali metals is extremely low, compared to selectivity for divalent alkaline earth metals. The results compiled in Table I indicate the SOMS phases could be used for applications such as 1) removal of radioactive Sr-90 from Na-rich wastes, 2) removal of radioactive Sr-90 from contaminated groundwater or soils containing high concentrations of Mg and Ca, and 3) cleanup of industrial waste

streams containing toxic metals including Cd^{2+}, Ni^{2+} or Zn^{2+}. We are particularly interested in applications involving the sequestration and immobilization of radioactive Sr-90.

In the interest of optimizing selectivity and exchange capacity of SOMS, thorough investigations of exchange mechanisms are ongoing. The Na1 and Na3 sites are coordinated to one and two water molecules respectively, and therefore are more likely to undergo ion exchange than the Na2 site which is coordinated to six framework oxygens. This supposition is verified by combined experimental and theoretical techniques. ICP-AES and X-ray powder diffraction (XRPD) analyses of H^+-exchanged SOMS-1 indicate that approximately 50% of the total sodium content exchanges for H^+ without disrupting the framework structure. The simulated powder pattern of SOMS-1 with half the Na1 atoms and all the Na3 atoms replaced by H^+ matches the observed XRPD pattern. Similarly, the XRPD pattern of 20% Sr^{2+}-exchanged SOMS-1 can be simulated by replacing half the atoms at the Na1 site with Sr^{2+}. These studies suggest that larger cations such as Sr^{2+} substitute into only the 6-coordinate Na1 sites. Since half Na1 can be removed while retaining the framework structure, the maximum predicted exchange capacity for Sr^{2+} on SOMS-1 is 25%, which is similar to the maximum observed exchange capacity of 20%.

Elemental analysis of 20% Sr^{2+} loaded SOMS-1 gave a final Na^+:Sr^{2+} ratio of 4:1, which exactly matches the framework Nb:Ti ratio. The ratio of the remaining sodium (unexchanged) to the niobium is 1:1, which indicates the Na^+ and Sr^{2+} exchange in a 1:1 ratio, since the initial Na:Ti:Nb ratio is 5:1:4. Therefore, in order to maintain charge balance, a H^+ from the framework hydroxyl is necessarily exchanged along with each Na^+:

$$Na^+ + H^+ \longleftrightarrow Sr^{2+} \qquad (1)$$

This is confirmed by the disappearance of the OH^- proton NMR resonance in Sr^{2+}-loaded SOMS-1 (+0.5 ± 0.5 ppm; observed only in unexchanged SOMS-1).

Finally, the Sr^{2+}-loaded SOMS-1 phase undergoes direct thermal conversion to a single-phase perovskite, which has a formula of $Na_4SrNb_4TiO_{15}$, and extremely low strontium PCT (product consistency test)[28] leach rates. The DTA-TGA analysis of the Sr^{2+}-loaded SOMS-1, along with micrographs of Sr^{2+}-loaded SOMS-1 and $Na_4SrNb_4TiO_{15}$ are shown in figure 3. The weight loss between 100 – 300 °C is dehydration followed by structure collapse. The exothermic phase change observed at 550 °C is associated with conversion to the perovskite form. The micrographs of the Sr^{2+}-loaded SOMS-1 and the $Na_4SrNb_4TiO_{15}$ perovskite reveal that this phase change takes place with minimal morphology change. This thermally-induced phase change provides a means of immobilizing hazardous metals (such as radioactive Sr^{2+}), after the metal is selectively removed from solution. Perovskite (titanate-based) is a major component in the well-known SYNROC ceramic waste form for high level radioactive waste storage.[13] The perovskite waste-form is known to be a reliable commodity for stability in radioactive fields and in repository conditions. Since the concentration of the exchanged-in strontium exactly matches that of the framework titanium, the perovskite formed upon calcination is charge balanced without oxygen vacancies[29] that might reduce the durability of the resulting phase. Additionally, alternative phases such as lamellar niobates, titanates, or titanoniobates[30] do not form. Finally, the low temperature required for this phase change, as well as the remarkable morphology preservation during this process indicates that remobilization of the strontium during heating is improbable.

This new family of SOMS with flexible framework chemistry provides a unique opportunity to investigate form-function relationships of materials with ion selectivity and exchange capabilities. The extraordinary divalent cation selectivity and a maximum exchange capacity which matches exactly the M^{IV} framework concentrations is likely to be a direct consequence of

the tunable substitution of the M^{IV} into the framework Nb^{V}. Additional material properties related to framework composition are currently under rigorous investigation, so that we may fully develop and understand the “tuneability” of these SOMS phases.

References:

6. Lehto, J. et al., Advanced Separation of Harmful Metals from Industrial Waste Effluents by Ion Exchange. *J. Radioanal. Nucl. Chem.* **208**, 435-443 (1996).
7. Mitchenko, T., Stender, P., Makarova, N., Optimization of Sorption Purification of Industrial Effluents, Waste Waters and Technological Solutions from Polyvalent Metal Ions. *Solvent Extraction and Ion Exchange* **16**, 75-149 (1998).
8. Clearfield, A. et al., Spherically Granulated Titanium Phosphate as Exchanger for Toxic Heavy Metals. *Waste Management*, **18**, 203-210 (1998).
9. Lehto, J. And Harjula, R., Selective Separation of Radionuclides from Nuclear Waste Solutions with Inorganic Ion Exchangers. *Radiochim. Acta* **86**, 65-70 (1999).
10. Sylvester, P. and Clearfield, A, The Removal of Strontium and Cesium from Simulated Hanford Groundwater Using Inorganic Ion Exchange Materials. *Solvent Extraction and Ion Exchange* **16**, 1527-1539 (1998).
11. Nenoff, T. M., Miller, J. B., Thoma, S. G., Trudell, D. E., Highly Selective Inorganic Crystalline Ion Exchange Materials for Sr^{2+} in Acidic Conditions. *Environ. Sci. Technol*. **30**, 3630-3633 (1996).
12. Anthony, R. G., Philip, C. V., Dosch, R. G., Selective Adsorption and Ion Exchange of Metal Cations and Anions with Silico-titanates and Layered Titanates. *Waste Management*, **13**, 503-512 (1993).
13. Anthony, R. G., Dosch, R. G., Gu, D., Phillip, C. V., Use of Silicotitanates for Removing Cesium and Strontium for Defense Waste. *Ind. Eng. Chem. Res*. **33**, 2702-2705 (1994).
14. Cheetham, A. K., Ferey, G., Loiseau, T., Open-Framework Inorganic Materials. *Angew. Chem. Int. Ed.* **38**, 3268-3292 (1999).
15. Ferey, G. The New Microporous Compounds and Their Design. *C. R. Acad. Sci*. **t. 1, Serie IIc**, 1-13 (1998).
16. Morris, R. E. and Weigel, S. J., The Synthesis of Molecular Sieves from Non-aqueous Solvents. *Chem. Soc. Rev*. **26**, 309-317 (1997).
17. Dosch, R. G., Northrup, C. J., Headley, T. J., Crystalline Titanate Ceramic Nuclear Waste Forms: Leaching and Radiation Damage. *J. Am. Ceram. Soc*. **68**, 330-337 (1985).

18. Li, L., Luo, S., Tang, B., Wang, D., Immobilization of Sodium-Bearing High-Level Radioactive Wastes in Synroc Containing (NaNd)TiO_3-type Perovskite. *J. Am. Ceram. Soc*. **80**, 250-252 (1997).

19. Luo, S., Li, L., Tang, B., Wang, D., Synroc Immobilization of High Level Waste Bearing a High Content of Sodium. *Waste Management* **18**, 55-59 (1998).

20. Nyman, M. et al., Integrated Experimental and Computational Methods for Structure Determination and Characterization of a New, Highly Stable Cesium Silicotitanate Phase, $Cs_2TiSi_6O_{15}$ (SNL-A) *Chem. Mater.,* **in press** (2000).

21. Donze, S., Montagne, L. Palavit, G., "Thermal Conversion of Heavy Metal Chlorides ($PbCl_2$, $CdCl_2$) and Alkaline Chlorides (NaCl, KCl) into Phosphate Glasses. *Chem. Mater.* **12**, 1921-1925 (2000).

22. Dyer, A. *An Introduction to Zeolite Molecular Sieves* (John Wiley & Sons, New York, 1988).

23. Nenoff, T. M. and Nyman, M. "A New Class of Inorganic Molecular Sieves: Sodium Niobium Metal Oxides" (Sandia National Laboratories Patent Technical Advance # SD-6576/S-93,849, Albuquerque, NM (2000)).

24. Rocha, J. et al., The First Synthetic Microporous Yttrium Silicate Containing Framework Sodium Ions. *Chem. Comm.*, 2103-2104 (1997).

25. Wenger, M., Armbruster, T., Crystal Chemistry of Lithium-Oxygen Coordination and Bonding. *Eur. J. Mineral*., **3**, 387-399 (1991).

26. Park, S. H., Daniels, P., Gies, H. RUB-23: A New Microporous Lithosilicate Containing Spiro-5 Building Units. *Microporous and Mesoporous Mat*. **37**, 129-143 (2000).

27. Nicolas-Tolentino, E., Tian, Z., Zhou, H., Xia, G., Suib, S. L., Effects of Cu^{2+} Ions on the Structure and Reactivity of Todorokite- and Cryptomelane-Type Manganese Oxide Octahedral Molecular Sieves. *Chem. Mater*. **11**, 1733-1741 (1999).

28. Luo, J., Zhang, Q., Huang, A., Giraldo, O., Suib, S. L., Double-aging Methods for Preparation of Stabilized Na-Buserite and Transformations to Todorokites Incorporated with Various Metals. *Inorg. Chem.* **38**, 6106-6113 (1999).

29. Luo, J., Zhang, Q., Suib, S. L., Mechanistic and Kinetic Studies of Crystallization of Birnessite. *Inorg. Chem.* **39**, 741-747 (2000).

30. Bedlivy, D., Preisinger, A., Die Kristallstruktur von $Na_2S[H_2O]_5$, $Na_2Se[H_2O]_5$ und $Na_2Te[H_2O]_5$. *Zeit. Krist*. **121**, 131-144 (1965).

31. Kunz, M., Brown, I. D., Out-of-Center Distortions Around Octahedrally Coordinated d(0) Transition Metals. *J. Solid State Chem.* **115**, 395-406 (1995).

32. Zheng, Z., Philip, C. V., Anthony, R. G., Ion Exchange of Group I Metals by Hydrous Crystalline Silicotitanates. *Ind. Eng. Chem. Res*. **35**, 4246-4256 (1996).

33. Mesko, M. G., Day, D. E., Immobilization of Spent Nuclear Fuel in Iron Phosphate Glass *J. Nucl. Mater*. **273**, 27-36 (1999).

34. Anderson, M. T., Vaughey, J. T., Poeppelmeier, K. R., Structural Similarities Among Oxygen-Deficient Perovskites, *Chem. Mater*. **5**, 151-165 (1993).

35. Fang, M., Kim, C. H., Mallouk, T. E., Dielectric Properties of the Lamellar Niobates and Titanoniobates $AM_2Nb_3O_{10}$ and $ATiNbO_5$ (A=H, K, M=Ca, Pb), and their condensation products $Ca_4Nb_6O_{19}$ and $Ti_2Nb_2O_9$. *Chem. Mater*. **11**, 1519-1525 (1999).

Methods

Synthesis of SOMS-1. Titanium (IV) isopropoxide (TIPT, 0.8 g, 2.8 mmol) and niobium (V) ethoxide (3.56 g, 11.2 mmol), and sodium hydroxide (6.7 g, 167.5 mmol) were combined in 40 ml deionized water in a 125 ml teflon liner for a Parr reactor and stirred vigorously. The final molar ratio of water:Na:Ti:Nb of the precursor mixture was 160:12:0.2:0.8, and the pH = 13.6. The mixture was reacted in a 175 °C oven for 5 – 7 days. Approximately 2.2 grams (93% yield based on TIPT) of white, microcrystalline powder was collected by filtration. Elemental analysis: Nb, 46.5 wt. % found, 46.3 wt. % calculated. Na, 13.8 wt. % found, 14.3 wt. % calculated. Ti, 5.5 wt. % found, 6.0 wt. % calculated.

Single-crystal X-ray diffraction data for $Na_{16}Nb_{12.8}Ti_{3.2}O_{44.8}(OH)_{3.2}\bullet 8H_2O$ were collected at 293 K on a Bruker SMART Platform charge couple device (CCD) diffractometer at the X3A1 beamline of the National Synchrotron Light Source (NSLS), Brookhaven National Laboratories (BNL), Upton NY, USA. Data are as follows: monoclinic *C*2/*c* (no. 15); a = 16.940 (3) Å, b = 5.033 (5) Å, c = 16.466 (3) Å; β = 114.00 (3)°, Z = 8, V = 1282.6 (3) Å^3, d_{calc} = 3.238 mg/m^3; μ = 3.351 mm^{-1}, 7.7° < 2θ (synchrotron radiation, λ = 0.643 Å) < 46.44°; total reflections = 2625 ; unique reflections = 1177; R[I>2σ(I)]=0.0629, R_w[I>2σ(I)]=0.1609; R(all data)=0.0687, R_w(all data)=0.1637;

GooF=1.004. All initial attempts to index the unit cell using the standard SMART [Siemens, SMART. Area Detector Control Software, Siemens Analytical X-ray Instruments Inc., Madison, WI, USA, 1994.] indexing routine failed. The specimen was indexed as a non-merohedral reflection twin, following the complete data collection, using the *GEMINI* suite of programs [V. G. Young, R. A. Sparks, *Acta Cryst. B* **in prep**. 2000]. The orientation matrices for two twin components were determined from a set of 431 reflections. The two orientation matrices are related by the following twin law (by rows) in reciprocal space: (-100; 0-10; 001). The integration program SAINT [Bruker, SAINT: Program to Integrate and Reduce Raw Crystallographic Area Detector Data, Bruker AXS, Inc., Madison, WI, USA, 1996] was used to generate two files of integrated intensities from the original frames of data. The structure was solved by SHELXS using data files generated using only the major twin component. The refinement of this file using SHELXTL [G. M. Sheldrick, SHELXTL, Bruker AXS Inc., Madison, WI, USA, 1997.] resulted in a poor refinement with R(F) = 0.132, high estimated standard deviation, and unreasonable bond distances to oxygen around Nb/Ti- and Na- sites. Consequently, the as-collected data was modified by assigning batch scale factors (BASF) to the overlapped utilizing the program Twin HKL. This generated a file in which allowance was made for both exactly overlapped reflections and partially overlapped reflections.

Instrumentation Differential Thermal Analysis-Thermogravimetric Analysis (DTA-TGA) experiments were performed on a STD 2960 TA DTA-TGA instrument with alumina as a standard for DTA. Samples (10 - 15 mg) were heated at 5 °C/min to 1000 °C with an argon flow of 20 cc/min. ^{1}H solid-state NMR was performed on a Chemagnetics CMS-300 spectrometer using a 5 mm Chemagnetic CRAMPS probe. The Br-24 pulse sequence was used to remove dipolar couplings. Magic Angle Spinning was applied to remove chemical shift anisotropy effects. The ^{1}H 90° pulse lengths were 1.6 μs and τ = 3.1 μs. Multiple pulse tune up procedures were followed and resolution was tested on adipic acid. Spinning speeds were all set for 1.8 kHz. ^{23}Na MAS NMR experiments were run at 130 MHz on a Bruker DRX-500 spectrometer using a 4 mm MAS probe. Spinning speeds were set to 12 – 14 kHz. All chemical shifts were referenced to 0.1 M NaCl solutions. Excitation pulses of π/20 (1μs) and delays of 4 s were used. Deconvolutions were performed by individually fitting each spectrum to a linear combination of one narrow Gaussian peak (octahedral site) and one second order Quadrupolar broadened central transition. X-ray powder data ($5° < 2\theta < 80°$, step size 0.01°, T = 298 K, λ = 1.3997 Å) for $Na_{16}Nb_{12.8}Ti_{3.2}O_{44.8}(OH)_{3.2}\cdot 8H_2O$ were collected on beamline 2.3 at the Synchrotron Radiation Source, Daresbury Laboratory, Warrington, UK. Rietveld refinement was carried out with GSAS [A. C. Larson, R. B. Von Dreele, Los Alamos National Laboratory, New

Mexico, USA] using the single crystal structural parameters as a starting model. There were no impurity or unexplained peaks in the pattern. The refinement, using a pseudo-Voigt peak-shape model, proceeded satisfactorily to yield refined parameters as follows: monoclinic, *C*2/*c* (no. 15), *a* = 16.9397 (4) Å, *b* = 5.0335 (2) Å, *c* = 16.4659 (5) Å; β = 113.998 (1)°, *V* = 1282.60 (7) Å^3, *Z* = 8, 58 variables, 565 contributing reflections, $R(F^2)$ = 0.1319, R_p = 0.1183, R_{wp} = 0.1495.

Acknowledgements:

The work carried out at SUNY was supported by the NSF through grant DMR-9713375. A.T. and J.B.P. (SUNY) thank Dr. R. A. Sparks (Bruker-AXS Inc.) and V. G. Young, Jr. (X-ray Crystallographic Facility, Department of Chemistry, University of Minnesota, Minneapolis) for their helpful discussions regarding twinning in SOMS-1. Research carried out in part at the NSLS at BNL is supported by the U.S. Department of Energy, Division of Materials Sciences and Division of Chemical Sciences, Office of Basic Energy Sciences (Grant DE-FG02-86ER45231).

W.T.A.H. thanks the EPSRC for provision of beam time through the DARTS scheme and E. J. MacLean for experimental assistance.

M.N. and T.M.N. acknowledge the DOE Environmental Management Science Program (EMSP), project #27601 for funding for this work.

Sandia National Laboratories (M.N. and T.M.N.) is a multiprogram laboratory operated by Sandia Corporation, a Lockheed Martin Company, for the United States Department of Energy under Contract DE-AC04-94AL85000.

Figure Captions:

Figure 1. Scanning Electron Micrographs of SOMS-1 ($Na_{16}Ti_{3.2}Nb_{12.8}O_{44.8}(OH)_{3.2}\bullet 8H_2O$), demonstrating variation in crystal morphology with varying ratio of Nb:Ti alkoxides in the precursor mixture. An increase in crystal size, along with a decreased aspect ratio is observed with increasing titanium alkoxide in the precursor mixture. (**A**) Ti alkoxide:Nb alkoxide = 1:4. (**B**) Ti alkoxide:Nb alkoxide = 1:3. (**C**) Ti alkoxide:Nb alkoxide = 1:2.

Figure 2. Polyhedral representation of the structure of SOMS-1 projected along the *b*-axis. The double chains containing disordered Ti/Nb (blue) centered octahedra are connected to two layers of six coordinated Na-centered polyhedra (yellow). Na3 in distorted square planer geometry is shown as a ball and stick model (water, blue; oxygen, red; Na, yellow).

Figure 3. Thermal conversion of Sr^{2+}-loaded SOMS-1 to $SrNa_4TiNb_4O_{15}$ perovskite. (**A**) DTA-TGA analysis of Sr^{2+}-loaded SOMS-1. Weight loss (TGA curve) up to 150 °C is surface water, and from 150 – 350 °C is internal, Na-bonded water (~ 5 wt. %). The exothermic phase change (DTA curve) observed at 575 °C is alteration to a perovskite phase, as confirmed by powder XRD. Scanning Electron Micrographs of Sr^{2+}-loaded SOMS-1 (**B**) and $SrNa_4TiNb_4O_{15}$ perovskite (**C**), showing virtually no morphology change accompanying this phase change.

Table I. Selectivity (K_d) of Metals on SOMS Phases

metal	20%-Na/Nb/Ti-SOMS (K_d, ml/g)	12%-Na/Nb/Zr-SOMS (K_d, ml/g)
Ba^{2+}	> 99,800	> 99,800
Sr^{2+}	> 99,800	> 99,800
Ca^{2+}	2300	2660
Mg^{2+}	230	460
Pb^{2+}	66,500	22,000
Cr^{3+}	> 99,800	> 99,800
Co^{2+}	> 99,800	> 99,800
Ni^{2+}	> 99,800	> 99,800
Zn^{2+}	> 99,800	> 99,800
Cd^{2+}	> 99,800	> 99,800
Cs^{+}	150	170
K^{+}	95	150
Li^{+}	8	35